Cretaceous Research 151 (2023) 105621

Contents lists available at ScienceDirect

Cretaceous Research

journal homepage: www.elsevier.com/locate/CretRes

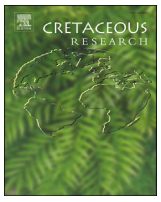

A new lower Turonian mosasaurid from the Western Interior Seaway and the antiquity of the unique basicranial circulation pattern in Plioplatecarpinae

Michael J. Polcyn [a, b, *], Nathalie Bardet [c], L. Barry Albright III [d], Alan Titus [e]

[a] Faculty of Geosciences, Utrecht University, Princetonlaan 8a, 3584, CB Utrecht, the Netherlands
[b] Huffington Department of Earth Sciences, Southern Methodist University, 3225 Daniel Ave., Dallas, TX 75275, USA
[c] CR2P – Centre de Recherche en Paléontologie de Paris, UMR 7207 CNRS-MNHN-SU, Département Origines et Evolution, Muséum national d'Histoire naturelle, CP38, 57 rue Cuvier, F-75005, Paris, France
[d] Department of Physics, University of North Florida, 1 UNF Dr., Jacksonville, FL 32224, USA
[e] Bureau of Land Management-Paria River District, 669 S. Highway 89A, Kanab, UT 84741, USA

ARTICLE INFO

Article history:
Received 4 November 2022
Received in revised form
30 May 2023
Accepted in revised form 7 June 2023
Available online 14 June 2023

Keywords:
Plioplatecarpinae
Tylosaurinae
Turonian
Mosasauridae
Tropic Shale

ABSTRACT

We describe and name a new mosasaur taxon, *Sarabosaurus dahli* gen. et sp. nov., from the lower Turonian part of the Tropic Shale in Utah, USA. The holotype specimen preserves significant portions of the skull and axial postcranial skeleton. It was found in the upper part of the *Watinoceras devonense* Ammonite Zone, bounded by radioisotopic dates above and below, and is thus about 93.7 Ma, the oldest mosasaurid taxon known from the Western Interior Seaway. The new taxon possesses a vascular pattern of the basisphenoid heretofore only seen in late diverging plioplatecarpine mosasaurids. Reevaluation of the morphology of the basisphenoid of previously described Turonian mosasaurs using μCT techniques reveals the derived condition is also present in *Yaguasaurus* and the incipient condition in *Tethysaurus* and *Russellosaurus.* In these two taxa, the canals enter the basisphenoid, but do not pass into the basioccipital. Instead, they exit only high on the posterior wall of the sella turcica, in a position similar to the basilar artery of other lizards. This vascular pattern, both in its incipient and derived states, is unique among squamates and supports inclusion of the aforementioned taxa in a monophyletic Plioplatecarpinae, for which we provide an emended diagnosis. Phylogenetic analysis recovers *Sarabosaurus dahli* gen. et sp. nov. as the sister taxon to *Yaguarasaurus* and all other later diverging plioplatecarpines, with *Russellosaurus* and *Tethysaurus* as successive sister taxa. Tylosaurine mosasaurids retain the primitive condition of the basisphenoid vascularization pattern and implies a tylosaurine-plioplatecarpine divergence in the late Cenomanian or earliest Turonian.

1. Introduction

Our understanding of mosasauroids has significantly advanced in the past few decades fueled by new discoveries and the restudy of historical specimens from the Cenomanian (100.5–93.9 Ma) and Turonian (93.9–89.4 Ma; Gale et al., 2020), revealing a diverse and complex early evolutionary history of the group (Bell, 1997; Paramo, 1994, 2000; Caldwell et al., 1995; Polcyn et al., 1999; Bardet et al., 2003; Polcyn and Bell, 2005; Bell and Polcyn, 2005; Dutchak and Caldwell, 2006; Caldwell and Palci, 2007; Smith and Buchy, 2008; Dutchak and Caldwell, 2009; Makádi et al., 2012; Palci et al., 2013; Polcyn et al., 2022). However, differences in the hypothetical relationships of these basal branching forms persist, placing many of the Turonian taxa in various arrangements with Tylosaurinae and Plioplatecarpinae, but not including them within those subfamilies (Polcyn and Bell, 2005; Caldwell and Palci, 2007; Makádi et al., 2012; Palci et al., 2013). Differences in the composition of character taxon matrices among these studies largely accounts for the varying topologies recovered. However, incomplete preservation, the plesiomorphic nature of the Turonian taxa involved, and analytical techniques employed in these previous studies failed to identify characters that unambiguously unite them with or exclude them from

* Corresponding author. Current Postal Address–Michael J. Polcyn, Huffington Department of Earth Sciences, Southern Methodist University, 3225 Daniel Ave., Dallas, TX 75275, USA.
E-mail addresses: m.j.polcyn@uu.nl (M.J. Polcyn), nathalie.bardet@mnhn.fr (N. Bardet), lalbrigh@unf.edu (L.B. Albright), atitus@blm.gov (A. Titus).

https://doi.org/10.1016/j.cretres.2023.105621

inclusion in higher level taxa. For instance, Polcyn and Bell (2005) discussed the large number of characters that two of these Turonian taxa, *Russellosaurus* and *Yaguarasaurus,* share with Plioplatecarpinae, raising the possibility that those taxa were basal members of that subfamily. Although many of those characters diagnose, at least in part, Plioplatecarpinae as currently conceived (*sensu* Konishi and Caldwell, 2011), the large number of plesiomorphies shared among the more inclusive clade Russellosaurina (Polcyn and Bell, 2005), resulted in their phylogenetic analysis reconstructing Tylosaurinae as the sister taxon to Plioplatecarpinae, and the aforementioned Turonian taxa together with *Tethysaurus* as the sister clade to Plioplatecarpinae plus Tylosaurinae. Subsequent analyses, which included additional Turonian taxa, recovered different arrangements in their strict consensus trees, but again, with Tylosaurinae and Plioplatecarpinae as sister taxa, and that clade the sister taxon to (*Tethysaurus* (*Russellosaurus* + *Yaguarasaurus*)) plus Halisaurinae (Caldwell and Palci, 2007) or the sister taxa to the clade formed by (*Tethysaurus* + *Pannoniasaurus*) plus the polytomy (*Russellosaurus* + *Yaguarasaurus*+*Tethysaurus*) (Palci et al., 2013). This underscores the need to identify and document key character complexes that may resolve this situation. One such complex is the basicranium, but in particular, its vascularization patterns which are largely conserved across tetrapods (Rahmat and Gilland, 2014).

In the broadly conserved pattern, a branch of the internal carotid artery, the cerebral carotid, projects medially and emerges within the sella turcica. This artery supplies the anterior parts of the brain, and also projects a branch supplying the posterior brain via the so-called basilar artery. Mosasaurids in the subfamily Plioplatecarpinae differ from other mosasaurids (and all other squamates) in possessing canals that enter the basisphenoid anterolaterally, just below the abducens nerve exit, and dorsal to the internal carotid artery path. These canals trend posteromedially, converging to emerge as small foramina or a single foramen, just below the dorsum sellae, and in late diverging plioplatecarpines continues posteriorly as a canal within the basisphenoid, passing into the basioccipital and emerging posteriorly from the dorsal surface of the basioccipital (Camp, 1942; Russell, 1967; Rieppel and Zaher, 2000a). In addition to the *de novo* vascularization, plioplatecarpines also retain the broader pattern of a cerebral carotid branching from the internal carotid and emerging within the sella turcica. Dollo (1885) first recognized the unique vascularization in *Plioplatecarpus* discussing various potential homologies without reaching any conclusion. The cranial circulation of *Plioplatecarpus* was later described in detail by DeVillers (1943), and Camp (1942) described the vascularization in *Platecarpus.* Russell (1967) reviewed previous work and interpreted it as carrying only the basilar artery, and suggested that the jugal and/or lateral head vein passed on the lateral surface of the basisphenoid, evidenced as a groove present in many taxa. In any event, this novel circulatory condition is unique among mosasaurids and all other squamates and is thus a pivotal character with great potential in understanding the relationships of other Turonian taxa.

We report here the oldest mosasaur in North America, from the Cretaceous Western Interior Seaway (KWIS) from the lower Turonian part of the marine Tropic Shale of Utah. *Sarabosaurus dahli* gen. et sp. nov., possesses a unique basicranial circulatory pattern, uniting it with Plioplatecarpinae. We document the geological context and age of the specimen, provide an emended diagnosis of Plioplatecarpinae, and diagnose the new taxon. We then provide an osteological description of the specimen, and furthermore, we document the basicranial circulatory patterns in *Tethysaurus*, *Russellosaurus*, *Yaguarasaurus,* and select taxa across Mosasauridae, and discuss functional implications. We conclude with a phylogenetic analysis and discussion of implications.

1.1. Institutional abbreviations

BRV, -Paleontological Collections, National University of Colombia, Bogata, Colombia; FHSM VP, -Fort Hays Sternberg Museum Vertebrate Paleontology Collection, Hays, KS, USA; GLCA, -Glen Canyon National Recreation Area, Utah, USA; GSENM, -Grand Staircase-Escalante National Monument, Utah, USA; IRSBN, -Royal Institute of Natural Sciences, Brussels, Belgium; KUVP, - University of Kansas Vertebrate Paleontology Collection, Lawrence, KS, USA; MGUAN, -Museum of Geology Agostinho Neto University, Luanda, Angola; MNA, -Museum of Northern Arizona, Flagstaff, AZ, USA; MOR, -Museum of the Rockies, Bozeman, MT, USA; MNHN, -Muséum National d' Histoire Naturelle, Paris, France; MPPS, -Museum of Paleontology and Prehistory, S. Anna d'Alfaedo, Italy; NHMM, - Natuurhistorisch Museum Maastricht, Netherlands; NPS, -National Park Service, USA; SMU, -Shuler Museum of Paleontology, Southern Methodist University, Dallas, Texas, USA; TxVP, -Texas Vertebrate Paleontology Collections, University of Texas at Austin, Austin, Texas, USA; UCMP, -University of California Museum of Paleontology, Berkeley, CA, USA; UMNH, -Natural History Museum of Utah, Salt Lake City, UT, USA.

2. Field area and geological setting

The Tropic Shale is a mostly grey-colored marine unit that crops out extensively around the margins of the Kaiparowits Plateau (Titus et al., 2016, and references therein). It is the middle of the area's three Greenhorn cyclothemic units (Naturita Formation: upper Cenomanian; Tropic Shale: upper Cenomanian-middle Turonian; and Tibbett Canyon Member of the Straight Cliffs Formation: middle Turonian) and was deposited in a shallow muddy shelf environment near the western edge (Fig. 1A) of the KWIS (Petersen, 1969; Doelling, 1975; Doelling and Davis, 1989; Eaton, 1991; Dyman et al., 2002;Titus et al., 2016). Because it reflects maximum flooding and highstand conditions (Hattin, 1985), the Tropic Shale consists mostly of shale and mudstone with increasing sandstone content upsection resulting from falling sea levels near the end of the Greenhorn event. A robust record of marine reptiles has recently come to light in the Tropic Shale that includes marine turtles and pliosaurid and polycotylid plesiosaurs (Gillette et al., 1999; Albright et al., 2007a; Albright et al., 2007b; Albright et al., 2013). Mosasaurids were first documented from this unit by Albright et al. (2012) who noted the discovery of the specimen described herein.

Fragmentary, isolated mosasaurid remains have now been found at nine localities in the lower 100m of the Tropic Shale, all along the southern margin of the Kaiparowits Plateau, Kane County, Utah. Material from all but one of these sites consists of isolated vertebrae that will not be treated in this paper. However, one locality (GLCA 327) yielded enough of a single individual (UMNH VP 21800/GLCA 24271) to be specifically diagnosed as a new taxon, *Sarabosaurus dahli* gen. et sp. nov.. The type locality is in the Last Chance Canyon area of Glen Canyon National Recreation Area (GCNRA) on the east side of a small saddle and was found in February 2012 by H. Scott Richardson (original site number TROPIC 12-11; Fig. 1B). Material was spread out in a 28-m-long, 3-m-wide (at the bottom) fan geometry beginning at the saddle. In March 2012, all obvious surface material was collected and then the entire alluvial deposit below the saddle was dry screened through a 0.5 cm mesh by a joint National Park Service-Bureau of Land Management crew to recover additional buried material. No in situ material was recovered. Fortunately, nearly in-situ elements were found on the east edge of the saddle, allowing it to be unambiguously constrained to an interval between 2 and 4 m above the "C" bentonite (using terminology of Elder, 1991), or alternatively,

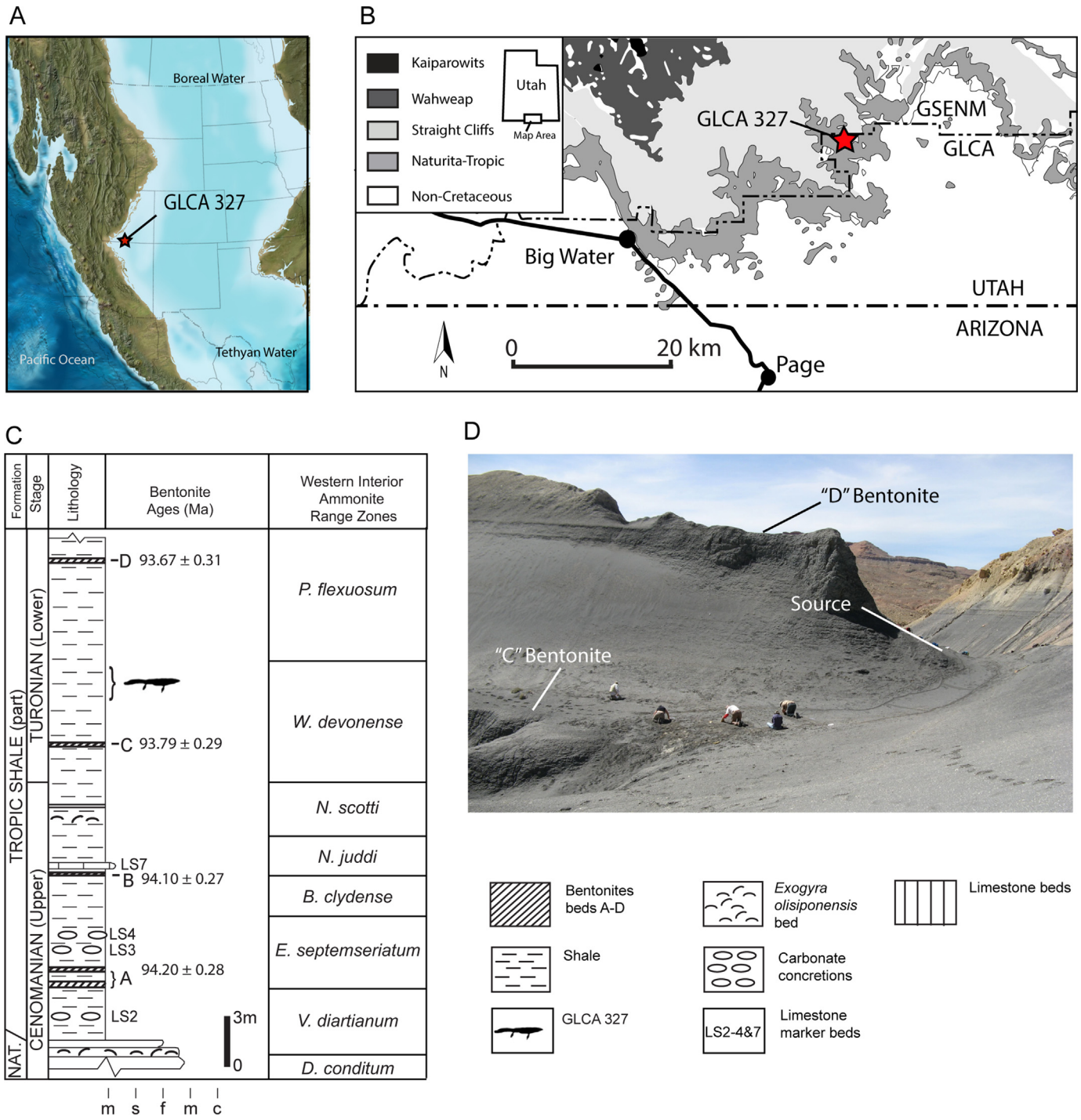

Fig. 1. (A) Turonian paleogeography with political boundary overlay showing site GLCA 327. (B) Reference map of study area along southern border of Kaiparowits Plateau. Finely dotted line separates Glen Canyon National Recreation Area from Grand Staircase-Escalante National Monument. Star denotes location of type specimen. Modified from Albright et al. (2007a). (C) Generalized stratigraphic column of GLCA 327. A, B, C, and D, are bentonites of Elder (1991). Abbreviations: LS, Limestone beds. Lim., Limonite bed, and approximate local stratigraphic position of Cenomanian-Turonian boundary. (D) GLCA 327 during recovery of (UMNH VP 21800/GLCA 24271), *Sarabosaurus dahli* gen. et sp. nov.. Base map in A licensed from Colorado Plateau Geosystems, Inc.

between 6 and 8 m below the "D" bentonite (Fig. 1C, D). This places the type specimen near or slightly below the base of the *Mytiloides kossmati* Inoceramid Biozone (Kennedy et al., 2005), which is equivalent to the boundary between the *Watinoceras devonense devonense* and *Pseudaspidoceras flexuosum* North American Ammonite Biozones (93.19 ± 0.42 Ma fide Cobban et al., 2006 or alternatively 93.38 ± 0.03 fide Sageman et al., 2006). Recent analysis of a core sample taken from the nearby SH1 borehole shows the interval between the "C" and "D" bentonites is about half the thickness of that at Last Chance Canyon, but confirms the biostratigraphic assignment (Jones et al., 2019). Figure 1A shows the placement of the site at ~93.7 Ma.

During the time associated with the *P. flexuosum* biozone, global sea levels were essentially at their highest point for the entire Cretaceous (Haq, 2014). Based on Cobban and Hook (1984) and Cobban et al. (1994), the east Laramidian shoreline of the KWIS was

located approximately 170 km west of locality GLCA 327 (Fig. 1A). Water depths were probably in the 75-100-m range (M. Leckie, personal communication, 2019), but incursions of warm Tethyan waters coupled with high productivity in the upper water column created dysoxic to anoxic conditions on the seafloor in what is regarded by most workers as a Tethyan-Boreal transitional zone (Elderbak and Leckie, 2016).

3. Systematic paleontology

Reptilia Linnaeus, 1758
Squamata Oppel, 1811
Mosasauridae Gervais, 1852
Russellosaurina Polcyn and Bell, 2005.
Plioplatecarpinae Dollo, 1884
Synonyms:
Plioplatecarpidae Dollo, 1884:653.
'mosasauriens microrhynques' Dollo, 1890:163.
Platecarpinae Williston, 1897:177.
Plioplatecarpini Russell, 1967:148.
Plioplatecarpinae Konishi and Caldwell, 2011.
Tethysaurinae Makádi et al., 2012.
Yaguarasaurinae Palci et al., 2013.

Included Genera— *Platecarpus* Cope, 1869; *Plioplatecarpus* Dollo, 1882; *Angolasaurus* Antunes, 1964; *Ectenosaurus* Russell, 1967; *Selmasaurus* Wright and Shannon, 1988; *Yaguarasaurus* Paramo, 1994; *Tethysaurus* Bardet et al., 2003; *Russellosaurus* Polcyn and Bell, 2005; *Latoplatecarpus* Konishi and Caldwell, 2011; *Plesioplatecarpus* Konishi and Caldwell, 2011; *Romeosaurus* Palci et al., 2013; *Gavialimimus* Strong et al., 2020.
Emended Diagnosis. (compare with Russell, 1967; Bell, 1997; Lingham-Soliar, 1994; Konishi and Caldwell, 2011); small to medium size mosasaurids (2–6 m); canals for basilar artery enter basisphenoid below abducens nerve exits and above internal carotid artery path, internally converging medially giving rise to the basilar artery, and in some taxa continue posteriorly within the basisphenoid and basioccipital, exiting on medullary floor of the basioccipital as paired canals or a single bilobate canal; premaxilla bears ventral median ridge just posterior to dentigerous portion; quadrate suprastapedial process elongate, reaching mid-height of quadrate in most taxa; two or three foramina on ventrolateral face of retroarticular process in most taxa; marginal tooth crown with sub-circular basal cross-section and medially finely striated, laterally faceted or fluted to various extent; parietal rami-supratemporal contact obliquely or horizontally oriented.
Remarks. The novel vascular pattern present in the basisphenoid of the *Sarabosaurus dahli* gen. et sp. nov. described herein is shared with *Tethysaurus*, *Russellosaurus*, *Yaguarasaurus*, and all other mosasaurid genera previously recognized as belonging to the subfamily Plioplatecarpinae (*sensu* Konishi and Caldwell, 2011). This vascular pattern is unique amongst mosasaurs and non-mosasaurian squamates and strongly supports the monophyly of this more inclusive arrangement to the exclusion of Tylosaurinae *contra* Konishi and Caldwell (2011), justifying the newly emended Plioplatecarpinae.

Sarabosaurus gen. nov.

Etymology. *Sarabosaurus* (Suh-raib-o-sawr-us) is derived from 'Sarab', an Arabic word meaning 'desert mirage' and the Greek 'sauros' meaning lizard. The 'lizard of the desert mirage' pays homage to the mirages often seen in the hot Tropic Shale badlands in the summer, which provided but a glimpse of the life that flourished in the long vanished Cretaceous Western Interior Seaway.
Type species. *Sarabosaurus dahli* gen. et sp. nov.
Diagnosis. The new taxon is diagnosed by the following unique combination of characters: premaxilla is anteriorly blunt, broadly arcuate in dorsal view with a small edentulous rostrum, ethmoid nerve enters premaxilla in a deep position, well below the dorsal surface and exits on dorsal surface as large irregularly spaced foramina, atavistic or paedomorphic retention of egg tooth, anterior internarial bar triangular in cross section; dermal sculpting present on the lateral face of maxillae; supradental portion of maxilla at external naris is transversely broader than tall; frontal supraorbital region is nearly square with dermal sculpting on the dorsal surface; prefrontal and postorbitofrontal separated by frontal supraorbitally, posterolateral alae of frontal rounded, posterior terminus of squamosal tear-drop-shaped without dorsal (parietal) process; relatively large lumina of semicircular canals; posteromedial vascular canal enters basisphenoid below abducens nerve exit, giving rise to basilar artery anteriorly and posteriorly forming a central vestibule within basisphenoid, pterygoid tooth row not elevated, sigmoidal, and bears at least 14 tooth positions, some of which are present on basisphenoid ramus; quadrate ventral body rostrocaudally thin, expanded ventral medial flange, small posterior 'infrastapedial' process, and poorly developed posteroventral ascending alar rim; dentary robust with small prow in front of first tooth position and medial ridge exposes nearly entire tooth root; tall well-developed median ridge on splenial; large zygosphenes present to at least the sacral vertebrae; depressed oval condyles on cervical and anterior trunk vertebrae, condyles on sacral and pygal vertebrae slightly taller than wide; anterior caudal vertebrae wider than tall; mid to posterior caudal vertebrae taller than wide.
Remarks. The nature of the angular-splenial articulation allows referral of the new taxon to Mosasauria (*sensu* Augusta et al., 2022) and the nature of the tooth implantation differentiates it from more basal mosasaurians, allowing referral to Mosasauridae (*sensu* Augusta et al., 2022). It can be excluded from both Mosasaurinae and Halisaurinae by the presence of articulating hemal spines which occurs in Russellosaurina. It shares with Plioplatecarpinae the triangular cross section of the posterior premaxillary ramus and the novel basisphenoid circulation. In comparison with other Turonian-age non-tylosaurine russellosaurian taxa which preserve cranial material, it can be differentiated from *Tethysaurus* by the advanced development of the dorsal part of the premaxilla and the morphology of the surangular anterior to the mandibular glenoid, both of which are shared with *Russellosaurus*. It can be excluded from both *Tethysaurus* and *Russellosaurus* by the rounded posterolateral frontal alae, and the posterior expansion of the internal basisphenoid circulatory vestibule. It can be further differentiated from *Romeosaurus* by the derived nature of the quadrate, significant development of a medial parapet on both the dentaries and maxillae, and the dimensions of the posterior part of the frontal, which is wider than long, in that taxon. In particular, the ventral portion of the quadrate in *Romeosaurus* is rostrocaudally thick in lateral view and the anteroventral tympanic rim rises in a more anterior direction, forming a more circular tympanic rim, more similar to *Russellosaurus*. *Sarabosaurus* can be differentiated from *Yaguarasaurus* by that taxon's relatively broad posterior frontal, significant development of a medial parapet on both the dentaries and maxillae, and a derived rostrocaudally expanded quadrate with a moderately developed posteroventral ascending tympanic rim.

Sarabosaurus dahli gen. et sp. nov.

(Figs. 2–12).

Holotype. UMNH VP21800 (GLCA 24271), fragments of cranium, mandible, and vertebrae representing cervical, dorsal, pygal, and caudal series.

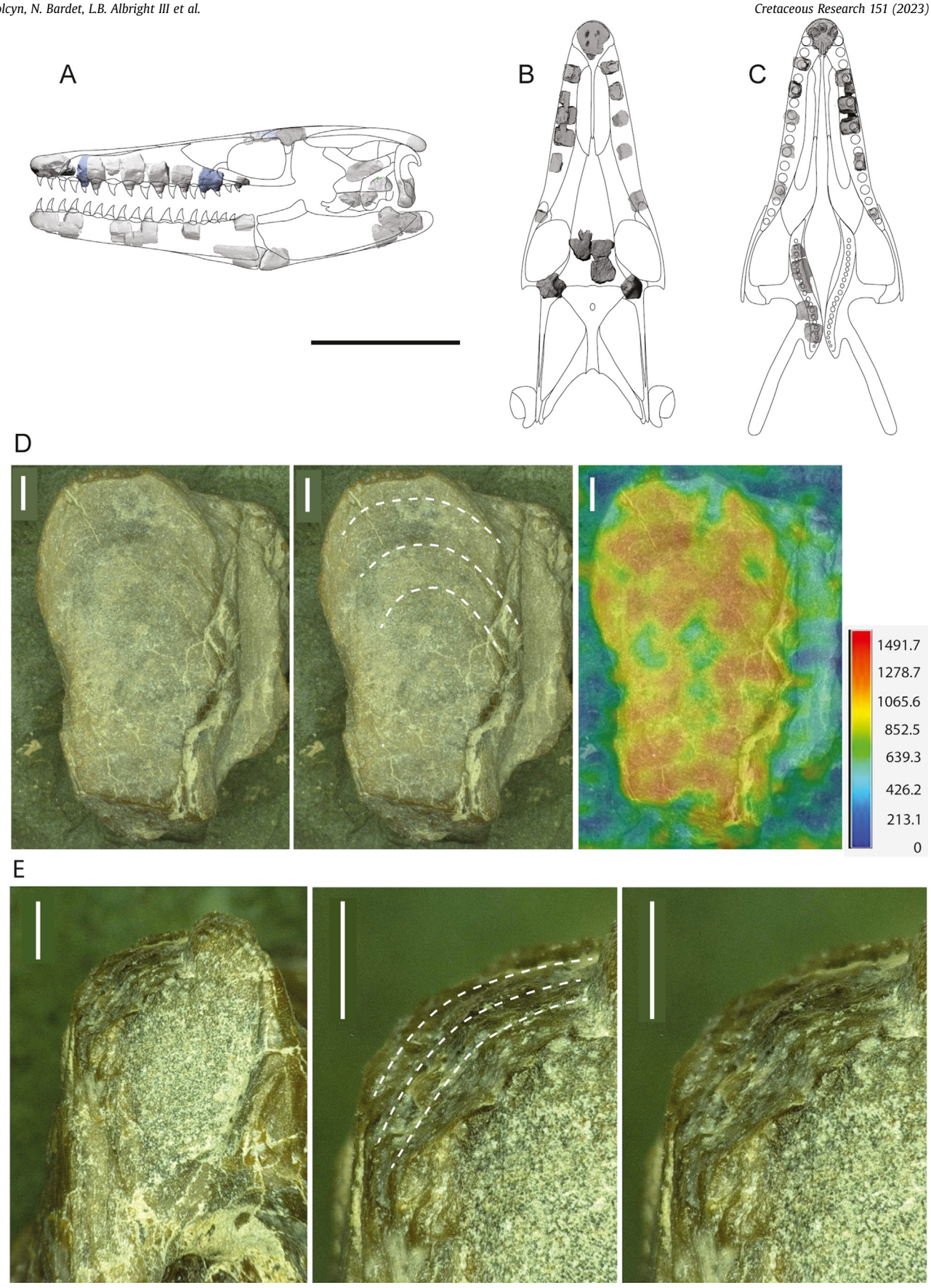

Fig. 2. Schematic reconstruction of the skull of *Sarabosaurus dahli* gen. et sp. nov. showing preserved elements in (A) lateral, (B) dorsal, and (C) ventral views. Some elements mirrored from opposite side. Reconstructed portions based on *Tethysaurus nopscai* (SMU75486) and *Russellosaurus coheni* (SMU73056). (D) Isolated zygopophysis showing growth rings with relative topographic relief shown in the third panel with legend given in microns, and (E), broken edge of zygosphene showing laminar bone deposition, interpreted as corresponding to annual growth. Scale bars equal 10 cm for A-C and 1 mm for D and E.

Type Locality. GLCA site 327, Glen Canyon National Recreation Area, Kane County, Utah, USA (detailed locality data on file at UMNH).
Etymology. The species epithet, *dahli*, is in honor of the many contributions of Steve Dahl, longtime volunteer at Grand Staircase-Escalante National Monument, Kanab, Utah.
Stratigraphic Occurrence. Lower part of the Mytiloides kossmati Inoceramid biozone, upper Pseudaspidoceras flexuosum North American ammonoid biozone.
Age. Early Turonian, bounded by radioisotopic dates on bentonites and constraining the horizon that produced the specimen to about 93.7 Ma.
Diagnosis. As for genus.

4. Description and comparisons

The following description is based on the holotype specimen (UMNH VP21800 [GLCA 24271]), which consists of a fragmentary skull (Fig. 2A-C) and a significant portion of the axial skeleton. We are confident the specimen represents a single individual, as marine amniotes are extremely rare in the Tropic Shale, most found as isolated elements, there are no anatomical elements repeated, some elements are still in articulation, and the preservation is consistent throughout the recovered portions. The individual would have measured approximately three meters in length, based on measurements of partial skeletons of *Tethysaurus* (SMU75486, and SMU76333). It does retain some articulation of vertebrae, suggesting the specimen may have been preserved in a fashion similar to other marine amniotes from this area prior to recent weathering (Albright et al., 2007a, 2007b). All elements have suffered some plastic deformation and recent weathering, rendering many of the elements fragmentary and surface preservation in some cases poor.

4.1. Ontogeny

The articulating surfaces and histology of zygosphenes and zygapophyses of squamates have been shown to preserve 'growth rings' which can be employed to determine the age of the animal (e.g., Venczel et al., 2015; Petermann and Gauthier, 2018). Recently, this method was applied to a halisaurine mosasaurid (Grigoriev et al., 2022). Using this method, the holotype specimen described herein (UMNH VP21800 [GLCA 24271]) is determined to be 3–4 years old, based on the pattern of 'growth rings' on the zygapophyses and also by discrete layers of laminar bone seen in broken zygosphenes (Fig. 2D, E). Additionally, surfaces of preserved cranial elements do not show a juvenile vascularization pattern, but instead exhibits bone surfaces that are finished and dense. There is a complete fusion of the exoccipital and opisthotic and no evidence of fontanels preserved on the basicranial elements nor the posterior frontal (Maisano, 2002, and references therein).

4.2. Premaxilla

The premaxilla is crushed and preserves only part of the dentigerous anterior portion (Fig. 3A-D) including three alveoli. In dorsal view, the anterior margin is broadly arcuate and blunt. Five large foramina are clearly visible on the preserved dorsal surface. The most anterior part of the premaxilla is smooth; however, fine

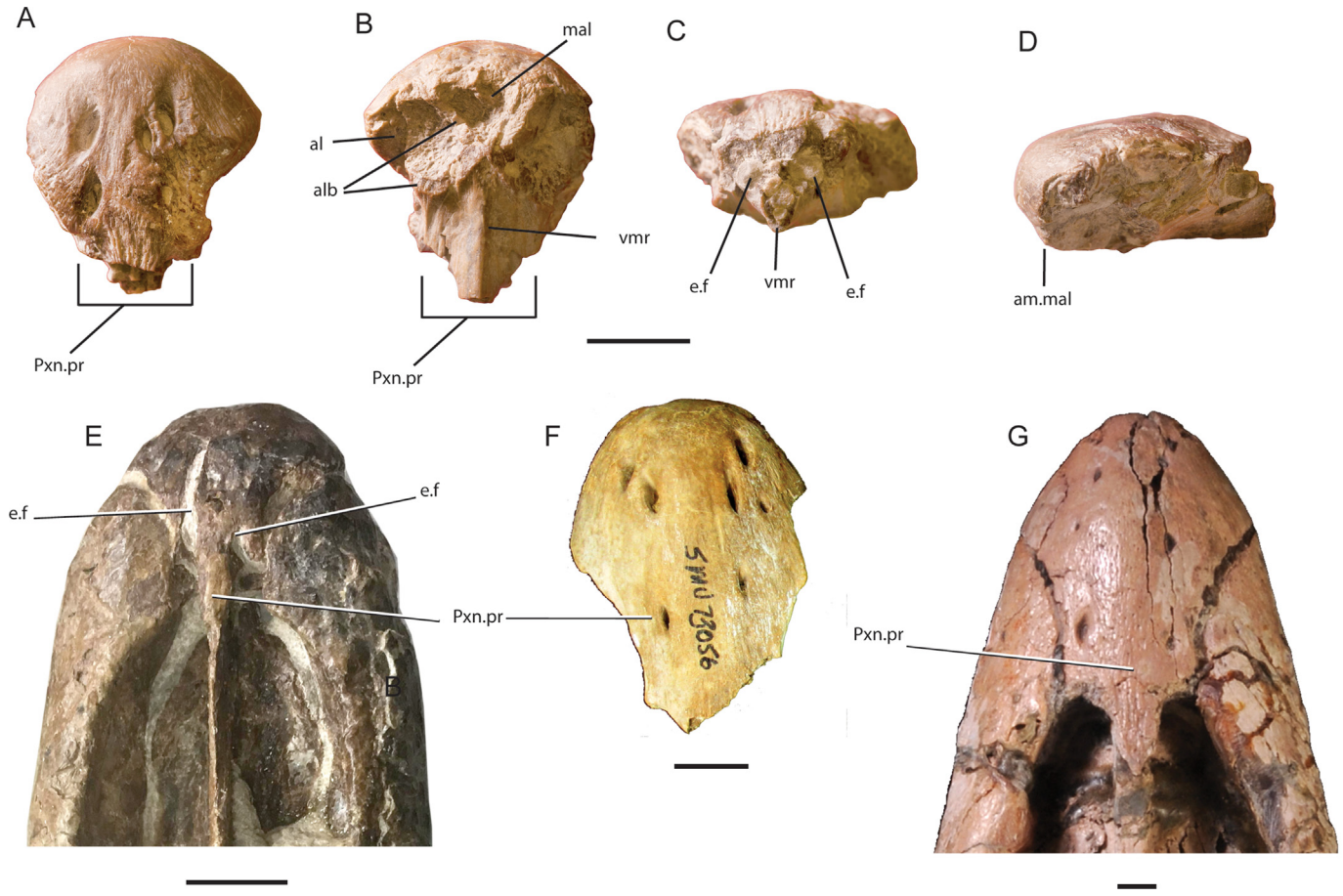

Fig. 3. Premaxilla of *Sarabosaurus dahli* gen. et sp. nov. in (A) dorsal, (B) ventral, (C) posterior, and (D) left lateral views. Anterior snout of *Tethysaurus nopscai* (SMU75486) in (E) dorsal view. Premaxilla of *Russellosaurus coheni* (SMU73056) in (F) dorsal view. Anterior snout of *Yaguarasaurus columbianus* (BRV-68) in (G) dorsal view. Abbreviations: al, alveolus; alb, alveolar bone; am.mal. anterior margin median alveolus; ef, ethmoid foramen; mal, median alveolus; pxn.pr, premaxilla nasal process; vmr, ventral median ridge. Scale bars equal 1 cm.

striae are present posteriorly on the dorsal surface becoming more pronounced on what would be the base of the internarial bar, a condition not seen in *Russellosaurus, Yaguarasaurus* or other more late diverging plioplatecarpines.

In ventral view a small portion of the premaxilla protrudes in front of the anterior alveolar margins. Three vacant alveoli are preserved, one median and two posterolaterally the posterior two alveoli are represented only by portions of their medial margins. The alveoli are distinct and form deep recesses, separated by a thin ridge of alveolar bone. The posterior alveoli would have been broadly separated by a field of finished bone, subrectangular posteriorly and triangular anteriorly, terminating on the posterior margin of the medial alveolus and bounded anterolaterally by the succeeding alveoli. There is no evidence of an elevated incisive process, and vomer processes are not visible; however, the posterior alveolar margins are worn and broken which may have precluded preservation. Posterior to the alveoli, the ventral surface bears a median ridge, weak anteriorly and posteriorly more pronounced, the cross-section of which is roughly triangular posteriorly. The condition is reminiscent of *Russellosaurus* (Polcyn and Bell, 2005) and of late diverging plioplatecarpines which possess a more vertically expanded ventral median ridge.

In posterior view, the entrance for the ophthalmic ramus of the fifth nerve is visible on the broken surface and filled with a resistant matrix (Fig. 3C), also present in maxillary, dentary, and braincase fragments. It enters in a relatively ventral position, parasaggitally, and at about mid-height, similar to *Russellosaurus* and most other mosasaurids, but unlike *Tethysaurus,* in which the path for the nerve is close to the dorsal surface of the premaxilla, in some cases exposing the posterior sulci dorsally. In lateral view, the premaxilla has a slightly inflated appearance, forming a short blunt rostrum, unlike *Russellosaurus.*

The premaxilla of *Sarabosaurus dahli* gen. et. sp. nov. is more derived than that of *Tethysaurus* (Bardet et al., 2003; Fig. 3E) and that of *Dallasaurus* (Polcyn et al., 2022) in that the dorsal surface in those taxa incompletely capture the ophthalmic ramus of the fifth nerve posteriorly, on the dorsal surface near the base of the narrow internarial bar. The posterodorsal part of the premaxilla in *Sarabosaurus dahli* gen. et. sp. nov. is more similar to *Russellosaurus, Yaguarasaurus* (Fig. 3F, G), and later branching plioplatecarpine taxa. *Eonatator sternbergi* (e.g., Lindgren and Siverson, 2005, their Figure 4) also displays posterior sulci on the dorsal surface near the base of the internarial bar, but the entrance for the fifth nerve is relatively deep. In the new taxon, the entrance is deep, well below the dorsal surface, and emerges as discreet foramina and the preserved portion suggest the posterior part would have been relatively wide. This condition is not necessarily phylogenetically useful, but does reflect a level of anterior narial retraction and upgrowth of the posterior part of the premaxillary-maxillary contact (Polcyn et al., 2022).

The median tooth position in the premaxilla may be homologous with the “egg tooth”, present *in-ovo* in most squamates (Anan'eva and Orlov, 2013), but retained in some mosasaurids that appear to be adult or subadult individuals. A median tooth is present in a basal halisaurine specimen (YPM 40383; Polcyn et al., 2022). A median tooth position is present in the premaxillae of two plioplatecarpines (TxVP 42942-2; SMU77681) and a new specimen of *Dallasaurus* from Texas (SMU76529), all from the Turonian of Texas. As would be expected, the premaxilla of an embryonic specimen of *Coniasaurus* sp. cf. *C. crassidens* (DMNH1601) collected with a gravid adult specimen also contains a median tooth (Polcyn et al., 2022). The appearance of a median tooth in the *Sarabosaurus dahli* gen. et sp. nov. described here, and the distribution of this unique character in what appear to be adult or subadult animals, may be due to paedomorphism, which appears to be common in secondarily adapted marine forms (Rieppel, 1993).

4.3. Maxilla

Parts of both maxillae are present (Fig. 4A–W), but extremely fragmentary, the largest piece preserving five tooth positions of the left maxilla. Tooth implantation is pleurodont, the bases ankylosed to the lateral wall and robust supradental shelf, which thins medially and wraps around the base of the roots forming a short medial ridge. Just lateral to the dorsal surface of the supradental shelf, within the lateral wall of the maxilla, runs the conduit for the maxillary artery and maxillary branch of the trigeminal nerve. Some fragments are broken as to expose a natural cast of these conduits, including those that emerge into foramina on the lateral face of the bone (Fig. 4X–Z), approximately at the interval of the tooth positions. Many of the fragments retain portions of the lateral bone surface, which has weak vermiform sculpting like that seen in the snouts of some mosasaurines (Fig. 4Z).

There are sufficient fragments to infer certain aspects of the snout morphology, but a faithful reconstruction is not possible. The premaxillary suture is not preserved, but two segments of the maxillae preserve portions of the narial margin. The more anterior of the two from the left maxilla (Fig. 4I–L) preserves the medial anterior exit for the maxillary artery (Fig. 4L). This exit lies dorsal to the posterior part of the fourth tooth position in *Russellosaurus* and *Tethysaurus.* A slightly more posterior portion of the right maxilla also preserves the dorsal margin of the external nares (Fig. 4O–S), together indicating a depressed anterior snout similar to that of *Tethysaurus*, with the height of the narial wall shorter than the width of the maxilla at that point.

The minimum maxillary tooth count is about 13 based on fragments that can be assigned to this bone; however, given the size disparity between the smallest and largest tooth bases, it appears quite a few tooth positions are not represented in the material and thus the tooth count may be higher. The maxillary tooth count in *Tethysaurus* is 19 or 20 (Bardet et al., 2003), in *Russellosaurus* sixteen (Polcyn and Bell, 2005), and in *Romeosaurus* fifteen (Palci et al., 2013). Around 12 or 13 is typical in late diverging plioplatecarpines.

In lateral view, the roots are clearly visible below the bony ventral margin, forming a weakly scalloped appearance at each tooth position. The medial ridge slightly embraces the bases of tooth attachment with a downturned lamina of bone, nearly exposing the entire base of the roots in medial view. The bony base of attachment is highly vascularized, its surface pierced by small foramina, and a small number (one to three) of larger foramina are seen at their bases, where they meet the supradental shelf.

No complete teeth are preserved, but the preserved tooth crown diameters at their bases are relatively small compared to the relatively large mass of attachment tissues. This condition is seen in *Haasiasaurus*, *Opetiosaurus*, *Aigialosaurus*, and *Tethysaurus,* taxa which possess relatively high tooth counts, and may merely reflect the plesiomorphic condition. Crowns are nearly circular in cross section and only small portions of the enamel are present, but show a very weakly striated texture. The tooth replacement inferred from breakage patterns suggests that every other tooth is in replacement (either missing or not fully ankylosed) with a mature, fully ankylosed tooth in between, though the precise phasing of the replacement waves is unclear. Resorption pits are posteromedial to medial in position, but no mature teeth show an advanced stage of resorption, suggesting replacement tooth growth largely occurred in the epithelial tissue.

4.4. Frontal

The frontal is fragmentary, missing most of the antorbital portion and left posterolateral portions (Fig. 5A–D). The right posterior margin is mostly preserved, but missing the posterolateral ala. There is prominent sculpting on the dorsal surface of the bone, composed

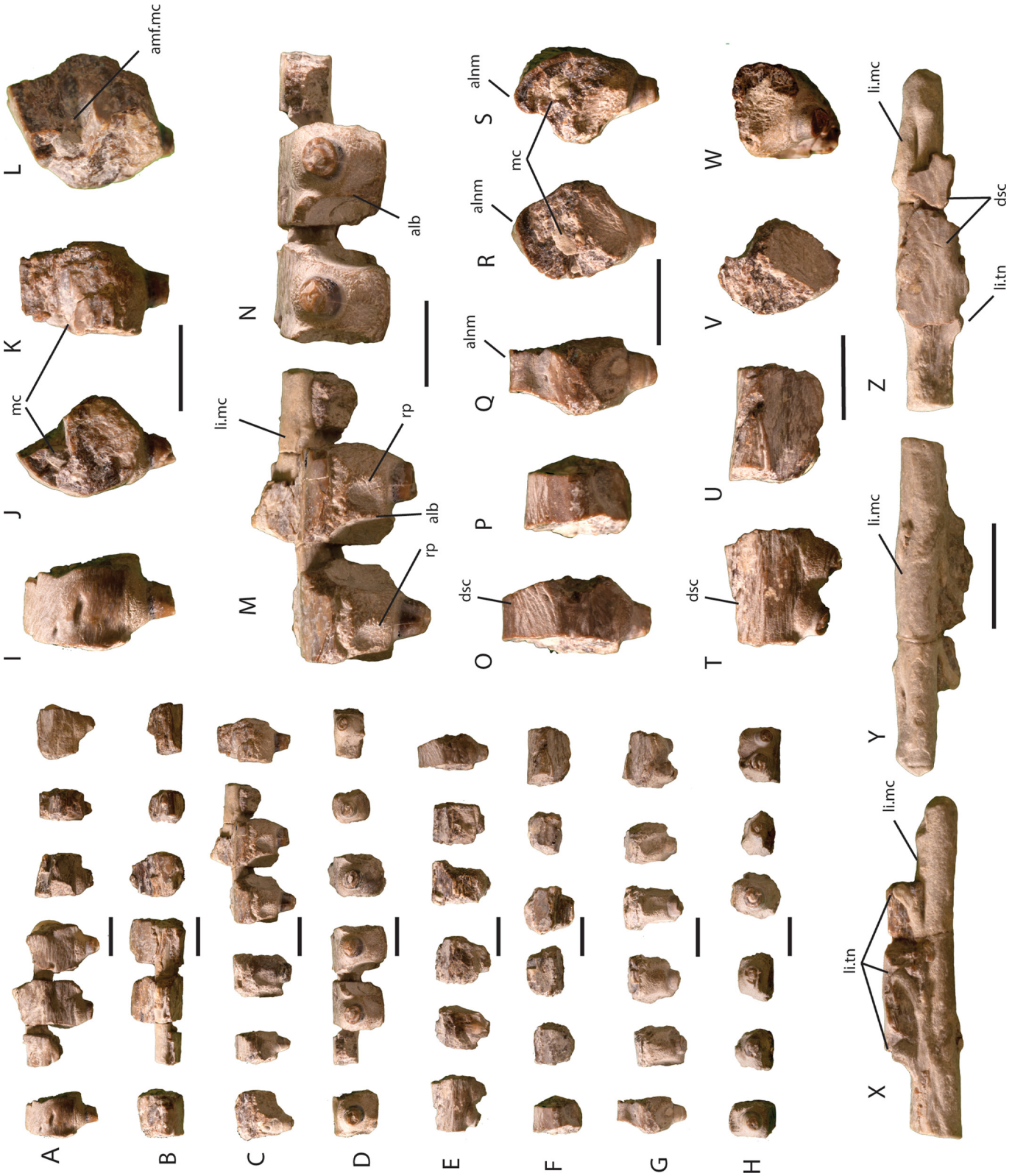
A
B
C
D
E
F
G
H
I
J
K
L
mc
amf.mc
M
N
li.mc
rp
alb
O
P
Q
R
S
dsc
alnm
mc
T
U
V
W
X
Y
Z
li.tn
li.mc
dsc

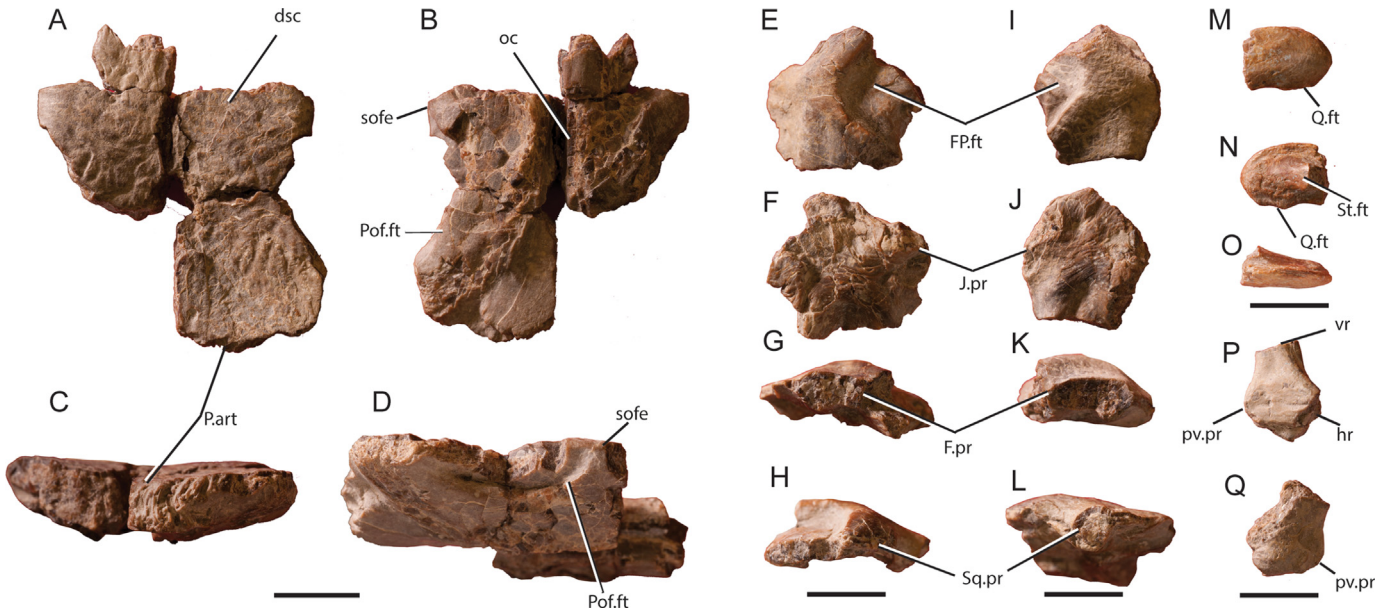

Fig. 5. Skull roof and suspensorium elements. Frontal of *Sarabosaurus dahli* gen. et sp. nov. in (A) dorsal, (B) ventral, (C) posterior, and (D) left ventrolateral views. Fragment of left postorbitofrontal in (E) dorsal, (F) ventral, (G) anterior, and (H) posterior views. Fragment of right postorbitofrontal in (I) dorsal, (J) ventral, (K) anterior, and (L) posterior views. Posterior fragment of left squamosal in (M) lateral, (N) medial, and (O) dorsal views. Posteroventral portion of left jugal in (P) lateral, and (Q) medial views. Abbreviations: fp.ft, frontoparietal facet; f.pr, portion of frontal process; hr, horizontal ramus of jugal; j.pr, base of jugal process; oc, olfactory canal; p.art, parietal articulation; pof.ft, postorbitofrontal facet; pv.pr, posteroventral process of jugal; sq.pr, portion of squamosal process; sofe, supraorbital frontal exposure; st.ft, supratemporal facet; vr, vertical ramus of jugal. Scale bars equal 1 cm.

of intersecting shallow grooves demarcating raised "islands" of bone. In ventral view, the frontal preserves the facet that receives the anterior ramus of the postorbitofrontal on the right side, anterior to which the lateral margin of the bone is complete, demonstrating separation of the prefrontal and postorbitofrontal supraorbitally. Taking the ratio of the midline length from the posterior prefrontal articulation to the frontoparietal suture compared to the interorbital width of the frontal, the frontal of *Sarabosaurus dahli* gen. et sp. nov. was relatively narrow and approximately square, as in *Tethysaurus* and *Russellosaurus,* and other more basal mosasauroids. In *Romeosaurus* (MPPS-45301) the supraorbital portion of the frontal is significantly wider than it is long. *Yaguarasaurus* is intermediate between the more basal forms and *Romeosaurus*.

The articular facet for the postorbitofrontal is relatively small as in *Russellosaurus* and *Tethysaurus*, restricted to the lateral third of the width measured from the midline to the lateral margin (Fig. 5B, D). A narrow parallel-sided olfactory canal lies anterior to a broad, subtriangular shield that would have roofed the cerebrum and is typically bounded anterolaterally by the bony sulci that received the planum supraseptale (the solium supraseptale); however, the sulci cannot not clearly be distinguished in the specimen described here due to crushing.

The posterior articulation for the parietal is bipartite (Fig. 5C). A medial, slightly concave portion with vertical comb-like sutural ridges covering the vertical thickness of the frontal, and more laterally, the sutural ridges progressively shift from vertical to dorsolateral covering the posterior face of a laterally thinning sheet of bone. Though not preserved in the specimen described here, in most other plioplatecarpines, there is a corresponding sheet of bone that originates on the ventrolateral part of the frontal. These two laminae form an oblique groove on the lateral part of the posterior face of the frontal into which a tab originating on the anterolateral part of the parietal would insert. This suture style is typical of non-tylosaurine russellosaurian mosasaurids, first reported by Bell (1997). The degree of sculpting on the dorsal surface of the frontal is remarkable and extremely rare in mosasaurids, and has only been reported in *Dallasaurus*, manifest as "broad, shallow, sublongitudinal ridges on the dorsal surface" (Bell and Polcyn 2005) and in some specimens of *Tethysaurus* (e.g. MNHN GOU 3; Bardet et al., 2003; their Figure 2A).

4.5. Postorbitofrontal

Both postorbitofrontals are present but badly damaged (Fig. 5E–L). The jugal, squamosal and anterior rami are broken on both. Articulation to receive the posterolateral process of the frontal is gently rounded, not angular as in *Tethysaurus* (Bardet et al., 2003), *Russellosaurus* (Polcyn and Bell, 2005), and *Yaguarasaurus* (Páramo, 1994), in which the frontal posterolateral alae are pointed and meet the postorbitofrontal (along with the parietal) in a more angular suture. The condition of the postorbitofrontal and its presumed conjugate relationship with the frontal and parietal in *Sarabosaurus dahli* gen. et sp. nov., is similar to the condition in some late diverging plioplatecarpines in which the frontal posterolateral alae are more rounded (e.g., *Plesioplatecaprus planifrons, Angolasaurus bocagei*), a condition also seen in a

Fig. 4. Maxillae of *Sarabosaurus dahli* gen. et sp. nov.. Left maxilla in (A) lateral, (B) dorsal, (C) medial, and (D) ventral views. Right maxilla in (E) lateral, (F) dorsal, (G) medial, and (H) ventral views. Detail of anterior section of left maxilla in (I) lateral, (J) anterior, (K) medial, and (L) posteromedial views. Fragment of anterior left maxilla in (M) lateral, and (N) ventral views. Fragment of anterior right maxilla in (O) lateral, (P) dorsal, (Q) medial, (R) anterior and (S) posterior views. Fragment of posterior right maxilla in (T) lateral, (U) dorsal, (V) anterior, and (W) posterior views. Infilled segments of the canal for the maxillary artery and trigeminal nerves and some adhering dermal bone in (X) ventral, (Y) dorsal, and (Z) lateral views. Abbreviations: alb, alveolar bone; alnm, anterolateral narial margin; rp, resorption pit; dsc, dermal sculpting; li.mc, lithified infill of maxillary canal for trigeminal nerve and maxillary artery; mc, maxillary canal; amf.mc; li.tn, lithified infill of trigeminal nerve exits (mental foramina). Scale bars equal 1 cm.

middle Turonian frontal of an unnamed taxon (KUVP 97200) reported by Polcyn et al. (2008; their Fig. 4A, B).

4.6. Squamosal

Only the posterior part of the left squamosal is preserved (Fig. 5M–O). Its posterior termination is a simple tear-drop shape in lateral view, with no ascending parietal process, a condition similar to *Tethysaurus* and *Russellosaurus* (Bardet et al., 2003; Polcyn and Bell, 2005). Posteriorly, there is a raised medial part, thickening anteriorly for supratemporal articulation, the anteroventral edge thicker than the anterodorsal edge. The medial surface is flat and lacks the longitudinal groove which receives a conjugate ridge on the supratemporal, as was reported for *Russellosaurus* (Polcyn and Bell, 2005). The ventral ridge may correspond to a similar structure in *Tethysaurus* which demarcates the ventral part of the supratemporal articulation. In *Tethysaurus* that ventral ridge slopes posteroventrally to meet the ventral border of the squamosal, unlike the specimen described here.

4.7. Jugal

A small fragment, tentatively identified as the jugal is present. It preserves only the posteroventral part and most of the horizontal and vertical rami are gone and no contact for the ectopterygoid is preserved (Fig. 5P, Q). The broken surface of the horizontal ramus is taller than wide and the vertical ramus nearly circular. The vertical and horizontal rami diverge at an angle of more than 90° and possesses a weak posteroventral process.

4.8. Pterygoid

Four discontinuous sections of the right pterygoid are preserved (Fig. 6A, B). There are two nearly adjacent sections, representing the part of the pterygoid anterior to the lateral divergence of the ectopterygoid ramus, and together preserve nine tooth positions. One section preserves the portion just posterior to the ectopterygoid ramus with two tooth positions and space for a third anteriorly. A fourth piece preserves a section of the basisphenoid ramus

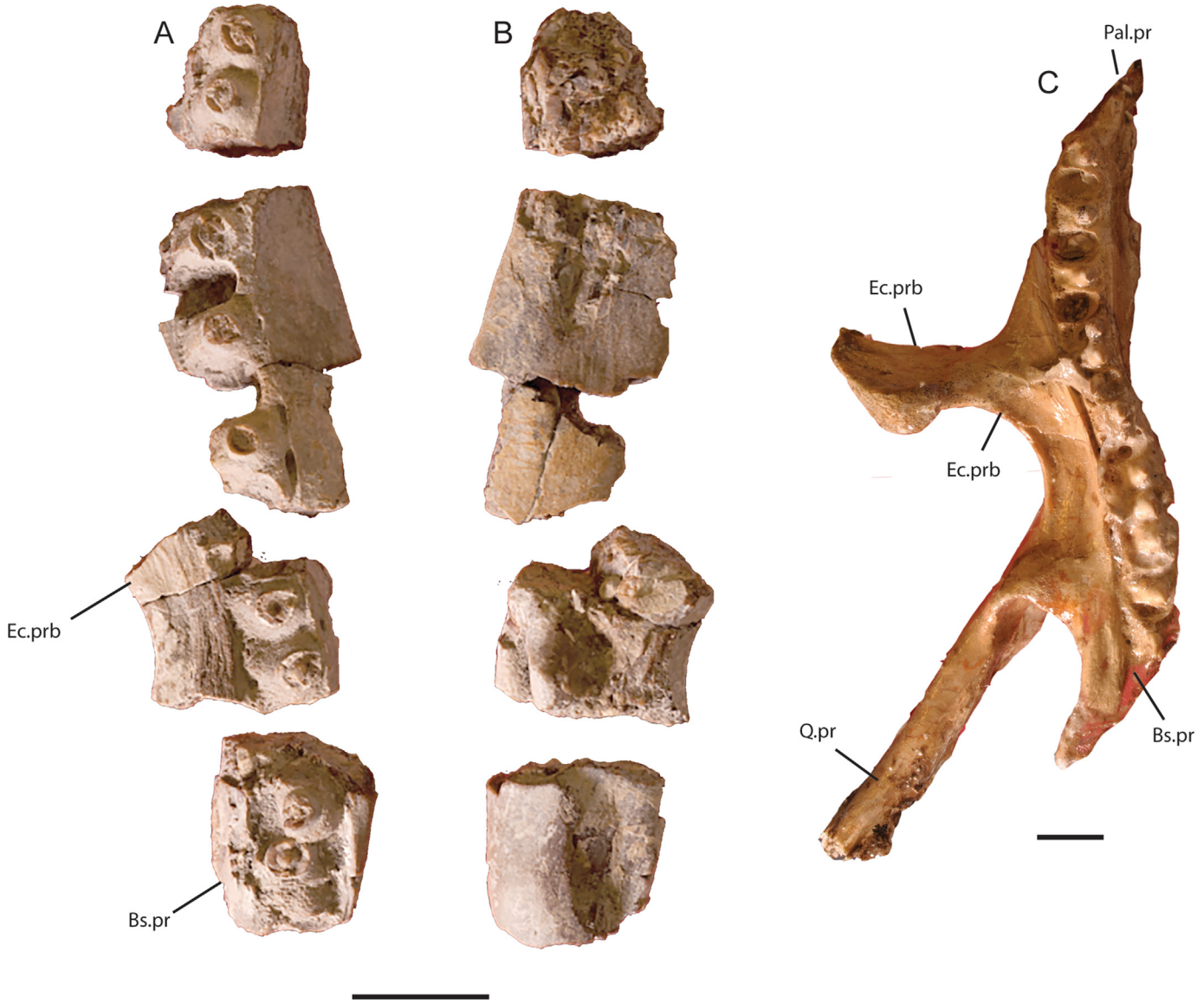

Fig. 6. Partial right pterygoid of *Sarabosaurus dahli* gen. et sp. nov. in (A) ventral and (B) dorsal views. Right pterygoid of *Tethysaurus nopscai* (SMU76334) in (C) ventral view for comparison. Abbreviations: bs.pr, basisphenoid process; ec.prb, ectopterygoid process base; pal.pr, palatine process; q.pr, quadrate process. Scale bars equal 1 cm.

with two tooth positions. Another tooth position anterior to this section is likely and an unknown number of tooth positions are not represented. The preserved sections represent a minimum of fourteen tooth positions and missing portions would have likely yielded a higher tooth count.

In dorsal view, the fossa to receive the basipterygoid process of the basisppenoid is visible posteromedially, and a fossa to receive the epipterygoid is prominent on the dorsal surface. A weak groove runs parallel to the lateral margin from anterior to the fossa and continues onto the ectopterygoid ramus.

In ventral aspect, the tooth row is slightly curved anteromedially as in other russellosaurians (straight in halisaurines and mosasaurines), and is not elevated (Bell, 1997, his char. 42:0) but arise from a transversely flat main body. Judging from the cross section of the tooth bases, the teeth are nearly circular, with the largest diameter in the middle and reducing in size both anteriorly and posteriorly. Tooth size is comparable to *Russellosaurus*, and relatively larger than in *Tethysaurus* which has very small pterygoid teeth. The teeth are ankylosed to the main body and medial wall with the lateral face of the roots broadly exposed anterolaterally and more concealed in the posterior section, where they sit within a shallow trough, beginning medial to the ectopterygoid process and continuing posteriorly. The medial wall of the tooth row slopes and broadens anteromedially, forming a sub-triangular profile in transverse section as in other plioplatecarpines. No obvious resorption pits are present on any tooth base.

In *Sarabosaurus dahli* gen. et sp. nov., the pterygoid possesses at least 14 tooth positions, while in *Russellosaurus* there are ten tooth positions with the posterior-most occurring medial to the posterior margin of the base of the ectopterygoid process, well anterior to the divergence of the basisphenoid and quadrate rami. The pterygoid in *Romeosaurus* (NHMV-V64108; Palci et al., 2013), though badly preserved, possesses at least 12 or 13 pterygoid teeth. There are 18 pterygoid teeth in *Tethysaurus* (Fig. 6C), and in other respects *Sarabosaurus* is quite similar to that taxon including the tooth row continuing posterior onto the basisphenoid ramus.

4.9. Basisphenoid

The basisphenoid is fragmentary, preserving only the dorsal parts of the element posterior to the sella turcica (Fig. 7A-E). In dorsal view, most of the medullary floor is preserved. It is broken anteriorly and anterolaterally, unroofing the canals for the abducens nerves, which are partially preserved as endocasts, infilled with a resistant material, similar to the vascular canal preservation of the dental rami. Anteromedially, between the abducens nerve endocasts, the posterior part of a large foramen is present, interpreted here as the foramen for the basilar artery (sensu Russell, 1967). The position of this foramen, high on the posterior wall of the sella turcia, is similar to the condition seen in *Russellosaurus* (Polcyn and Bell, 2005, their Figure 5F) in which the posterior part of the foramen meets the dorsum sellae. The foramen for the basilar artery in *Tethysaurus* is lower on the posterior wall of the sella turcica (described below). In later diverging plioplatecarpines, the basilar artery does send dorsal branches into the posterior part of the sella turcica near the dorsum sellae in some taxa, but the much larger paired vessels continue posteriorly internal to the basisphenoid, passing through the basisphenoid-basioccipital suture, and emerge on the posterior floor of the basioccipital.

The abducens nerves enter the floor in a lateral position and about half the distance between the posterior articulation for the basioccipital and the posterior rim of the anterior medial foramen (Fig. 7A). This position is relatively much further posterior than in either *Russellosaurus* or *Tethysaurus* and other plioplatecarpines examined. Anteriorly, the abducens paths diverge laterally and bend anteroventrally, but are truncated by breakage and the clinoid processes are not preserved. In dorsal view of the basisphenoid, at about the posterior terminus of the abducens entrance, is a small medial foramen, and more posterior to it, an additional three small paramedian foramina. Posteriorly and in dorsal view, the medial third of articulation with the basioccipital bears a shallow embayment with vertical sutural ridges. In dorsal view, lateral to the medullary trough of the basisphenoid, the articulations for the prootics are present but poorly preserved. They show a bipartite articulation; a vertical set of sutural ridges along the lateral wall of the medullary trough, and a ventrolaterally inclined shelf of smooth bone lateral to that (Fig. 7B).

The preserved posterior face of the basisphenoid can be divided between a prominent dorsomedian, suture-bearing region, offset slightly posteriorly from a flat featureless, anterodorsally inclined region, which is only preserved on the left side (Fig. 7C). The dorsal region is relatively complete, its dorsal margin (which is the profile of the posterior floor of the braincase in posterior view), forms a shallow concavity and the ventral margin of this region is broadly v-shaped, the two margins joined laterally by short, nearly vertical sides. The entire face of this region bears vertical sutural ridges, the deepest and most prominent toward the middle.

Most of the anterior and ventral parts of the basisphenoid are not preserved, exposing only an internal view of the main body of the basisphenoid (Fig. 7D, E). The foramen for the basilar artery opens ventrally into a chamber within the basisphenoid. The roof of this chamber preserves parts of anterolateral canals that would have exited the anterior basisphenoid slightly below the exits for the abducens nerves. These canals are interpreted here as the anterior branches of the basilar artery (sensu Russell, 1967), and remarkably, the chamber expands posteriorly as in later diverging plioplatecarpines. The canal is truncated posteriorly by breakage, but the preserved portion of the basioccipital suggests the basilar artery may have cross the basisphenoid-basioccipital suture. Possession of a posterior path for the basilar artery is markedly different from *Tethysaurus* and *Russellosaurus* in which the basilar artery exits in vertical canal at or just below the dorsum sellae, and does not continue posteriorly, communicating only with the anterolateral foramina; however, in *Russellosaurus*, the condition is less clear due to crushing and breakage (see descriptions below). Nonetheless, in both *Tethysaurus* and *Russellosaurus* the sella turcica is tall, rostrocaudally short, and a horizontal septum separates the vidian canal into a ventral part which carries the carotid artery and a dorsal part which carries the anterolateral part of the so-called basilar artery, above which is the exit for the abducens nerve. This anteriorly bifurcated vidian canal was previously noted by Rieppel and Zaher (2000a) in *Platecarpus*. In some late diverging plioplatecarpines such as *Latoplatecarpus willistoni*, the sella turcica is narrow and vertically reduced and the lateral wall of the vidian canal begins more posteriorly. Anteriorly, lateral to the sella turcica, two sulci are visible, separated by a weak lateral ridge. The ventral sulcus carries the palatine branch of the internal carotid artery and the dorsal sulcus the vessel which enters the basisphenoid and gives rise to the basilar artery.

In the specimen described here, in lateral view, there are long grooves just below the articulation for a lateral projection of bone that articulates with the prootics dorsally. Anteriorly the groove meets the anterolateral path of the basilar artery. This is like the condition in *Tethysaurus* in which the path inferred to be that of the internal jugular vein (lateral head vein of Russell, 1967) lies high on the lateral surface of the basisphenoid and intersects the anterolateral aperture of the basilar artery canal anteriorly (Fig. 7B). Posterolaterally, on the more complete left side, a second groove is visible just below the path of the internal jugular vein, and is likely the posterior part of the vidian canal.

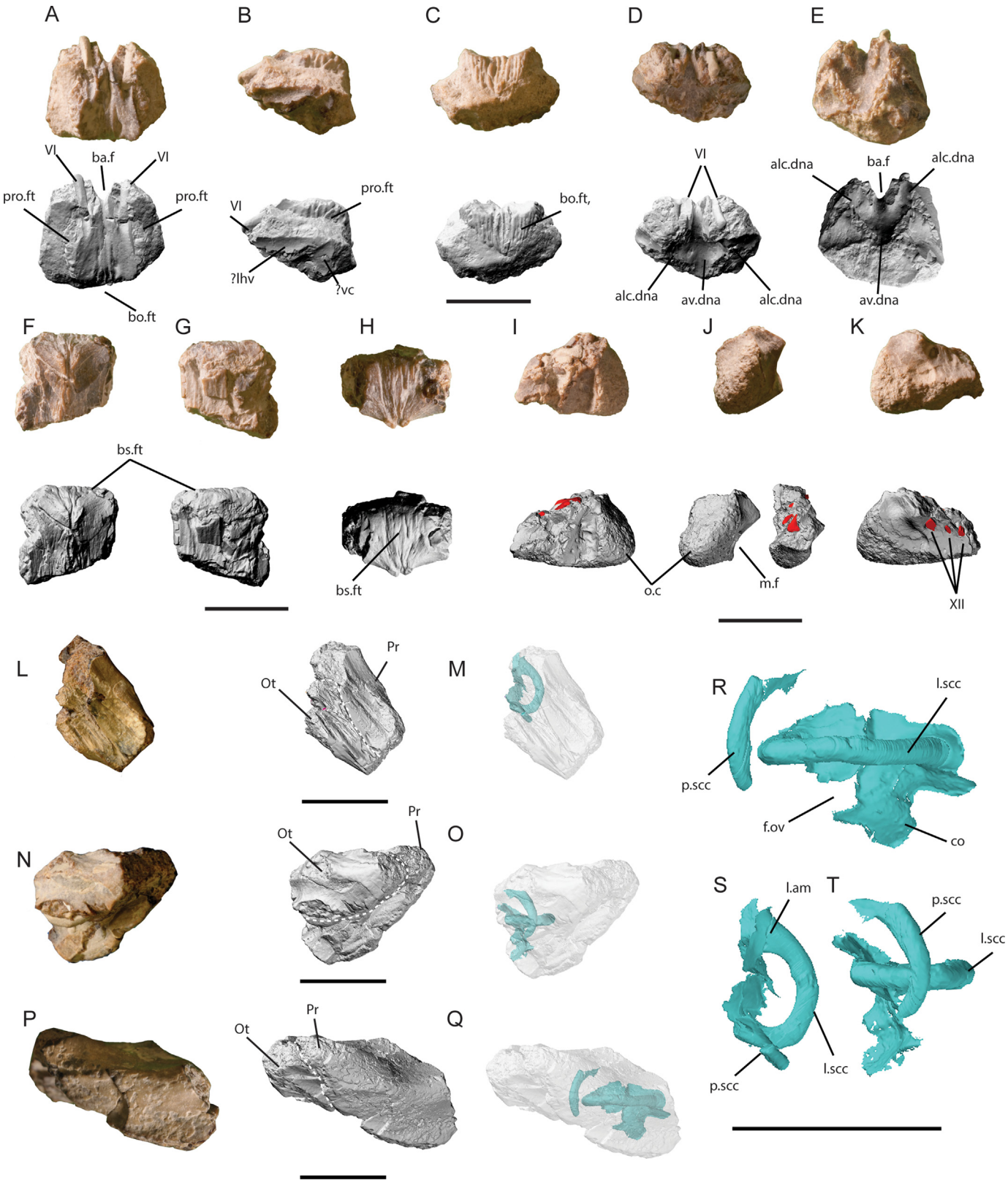

Fig. 7. Braincase elements of *Sarabosaurus dahli* gen. et sp. nov.. Dorsal portion of the basisphenoid in (A) dorsal, (B) left lateral, (C) posterior, (D) anterior, and (E) ventral views. Dorsomedial anterior portion of the basioccipital in (F) ventral, (G) dorsal, and (H) anterior views. Posteroventral portion of left otooccipital, in (I) lateral, (J) posterior, and (K) medial views. Partial right otooccipital in (L, M) dorsal, (N, O) medial, and (P, Q) lateral views. Details of partial endocast of the osseous labyrinth in (R) lateral, (S) dorsal, and (T) posterior views. Anatomical abbreviations: alc.dna, anterolateral canal for the de novo artery; av.dna, anterior vestibule de novo artery; avc, anterior vidian canal; ba.f, basalar artery foramen; bo.ft, basioccipital facet; bs.ft, basisphenoid facet; cca, cerebral carotid artery; co, cochlea; dna, de novo artery; f.ov, fenestra ovalis; l.scc, lateral semicircular canal; ot, otoccipital; pa, palatine artery; pcc, posterio cerebral carotid artery; pro.ft, prootic facet; p.am, posterior ampulla; p.scc, posterior semicircular canal; pr, prootic; VI, abducens nerve; XII, hypoglossal nerve; vc. vidian canal. Scale bars equal 1 cm.

4.10. Basioccipital

We interpret a small, rectangular bone fragment as the basioccipital (Fig. 7F-H). CT examination verifies cortical bone is covering three surfaces of the bone described here as the dorsal, ventral, and anterior surfaces. Crushing has caused numerous cracks and displacement on the dorsal surface, and some minor displacement of the ventral. The anterior surface appears largely undamaged, and is covered by weak vertical ridges, extending from the ventral surface to the dorsal margin, interpreted as the conjugate articulation for the basisphenoid. In anterior view, the element displays a median peak on its ventral margin, and its ventral surface displays a central ridge. The anterior terminus of the ridge is weakly bifurcated. The ridge may be somewhat exaggerated due to plastic deformation, but examination of CT data does not indicate displacement. This morphology may be evidence of the dorsal roof of a bilobate canal as seen in later diverging plioplatecarpines; however, incomplete preservation and crushing precludes certainty.

4.11. Otooccipital-Prootic

The otooccipitals and prootics are fragmentary (Fig 7I–Q). A small fragment of the right lateral wall of the braincase is preserved which includes portions of the co-ossified exoccipital and opisthotic, the otoccipital, and articulated prootic (Fig. 7L–Q). The anterior part of the prootic is broken posterior to and at about the level of the trigeminal notch and thus does not preserve the inferior or alar processes. Posteriorly, the prootic is broken near the posterior extent of the supraoccipital sutural surface. The preserved lateral face of the prootic is weakly concave anteriorly, the posterior expression of the trigeminal notch, as in other mosasaurids, and more vertically flat posteriorly. The ventral margin forms the lateral wall (the crista prootica of Oelrich, 1956) of an inverted u-shaped trough referred to here as the stapedial trough, which runs from the preserved posterior terminus, widening anteriorly, and terminates at the fenestra ovalis (Fig. 7N). In *Tethysaurus* the stapedial trough widens posteriorly but has a relatively well-developed crista prootica. In *Russellosaurus*, the crista prootica is less developed but forms a narrow ridge and in later diverging plioplatecarpines it is reduced to a low rounded ridge.

The preserved anterodorsal part of the prootic is thick and embraces the otoocippital medially forming a suture that transects the vestibule. Posteriorly, the prootic clasps the otooccipital between a thin, medially directed dorsal part and the main body of the posterior process laterally. The anterior part of the lateral face slopes dorsomedially to nearly horizontal, forming a rounded ridge, before sloping dorsomedially to form the broken base of the alar process. In dorsal view, the medial part of the prootic abuts the lateral supraoccipital sutural contact on the otooccipital. The medial lamina of the prootic overlying the otooccipital thickens anteriorly, sloping up to the base of the alar process. The transverse cross section of the preserved dorsal surface of the prootic is nearly horizontal posteriorly and inclined dorsomedially anteriorly as in both *Tethysaurus* and *Russellosaurus*. In later diverging plioplatecaprines it is more or less continuously dorsomedially inclined. The roof of the jugal foramen (*sensu* Russell, 1967; vagus foramen of Oelrich, 1956) is preserved medial to and at about the level of the oval window on the posteroventral surface of the preserved part of the otooccipital (Fig. 7O). It appears to be more broadly open posteriorly as in *Tethysaurus.* The jugal foramen is separated from the stapedial trough by a relatively thick wall, the posterior part of which is much thicker, suggesting *Sarabosaurus dahli* gen. et sp. nov. may have had a relatively thick crista tuberalis.

The medial and ventral parts of the bone are broken in such a way to expose the preserved portion of the osseous labyrinth including part of the vestibule, the lateral semicircular canal (SCC), and partial posterior SCC (Fig. 7R, S). The general shape and proportions of the vestibule is similar to later diverging plioplatecarpines (Georgi, 2008; Cuthbertson et al., 2015; Yi and Norell, 2018). However, *Sarabosaurus dahli* gen. et sp. nov. has relatively larger diameter lumina and the preserved ampulla is large and more pronounced. In later diverging taxa, the SCCs have relatively narrow diameter lumina and are nearly circular in shape (e.g., Georgi, 2008; Cuthbertson et al., 2015; Yi and Norell, 2018). The bony parts of the lateral and posterior SCCs do not intersect as in *Platecarpus* and *Plioplatecarpus*.

A second fragment of the left otooccipital preserves a small portion of the posterolateral braincase wall (not figured). The posteromedial surface is concave and corresponds to the broadest part of the foramen magnum. Posterodorsally, a low rounded ridge is present that would have roofed the posterolateral part of the foramen magnum to continue posterior as part of the parocciptial process. The dorsal part of this ridge abuts the supraoccipital laterally in dorsal view.

A third fragment of the braincase preserves the posteroventral part of the left otoccipital, including the condyle, and parts of the medial and lateral walls (Fig. 7I–K). The top part is truncated at about the ventral margin of the hypoglossal foramen posterolaterally, where the paths of all three branches can be partially seen in dorsal view of the broken surface. The medial wall is a bit higher preserving the posterior two foramina that would have carried the trunks of the nerves and the anterior trunk is exposed on the anteromedial broken surface. Together, the medial arrangement of the foramina and their position is as in other mosasaurids. On the medial wall, posteroventral to the posterior hypoglossal foramen, is a deep fossa, bounded medially by a sharp crest that is not present in either *Tethysaurus* or *Russellosaurus*.

A small anterolaterally facing surface, that parallels the path of the anterior hypoglossal nerve canal, is the remnant of the posterior wall of the occipital recess. The posterior face of the base of the crista tuberalis is preserved, but the crista itself is damaged. There is a lateral constriction anterior to the condylar surface and posteroventral to the hypoglossal nerve exits, that forms a relatively deep vertical sulcus, bounded anteriorly by the base of the crista tuberalis. The condylar surface is large, comparable to that in *Tethysaurus,* in which each side contributes about one-fifth of the contact area. In *Sarabosaurus dahli* gen. et sp. nov., the roof of the jugal foramen appears to be more broadly open posteriorly as in *Tethysaurus* while in *Russellosaurus* it is more narrowly oval, but some of this may be due to crushing.

4.12. Quadrate

Only the ventral part of the left quadrate is preserved (Fig. 8A–E). In dorsal view the broken cross section of the shaft is roughly triangular, with a slightly sigmoidal anterior margin and pointed posterior one, its apex at the dorsal part of a dorsomedial trending ridge on the posterior face, homologous to the so-called infrastapedial process of Russell (1967; Bell, 1997). In posterior view most of the surface is well preserved but there is a broken surface ventromedial to the infrastapedial process. Medial to the infrastapedial process, the posterior face trends anteromedially, but is broken distally. The relative thickness and trending direction suggest it would have formed an anterior ventromedially deflected flange, similar to condition in *Tethysaurus* (Fig. 8F–J) in which an anterior ventromedial flange accepts the quadrate ramus of the pterygoid in a deep facet (Fig. 8I, J). The condition in *Russellosaurus* (Fig. 8K–O) is similar but the receiving area is less deeply developed (Fig. 8N, O). Near the posterolateral margin, at about the level of the ventral extent of the pterygoid process, is a small tubercle we

Fig. 8. Partial right quadrate of *Sarabosaurus dahli* gen. et sp. nov. in (A) lateral, (B) posterior, (C) ventral, (D) medial, and (E) posterior views. Right quadrate of *Tethysaurus nopscai* (SMU76334) in (F) lateral, (G) posterior, (H) ventral, (I) medial, and (J) posterior views. *Russellosaurus coheni* (SMU73056) in (K) lateral, (L) posterior, (M) ventral, (N) medial, and (O) posterior views. G-O reversed for comparison. Abbreviations: avm.fl, anterior ventromedial flange; pt.pr, pterygoid process; pt.ft, pterygoid facet; pvr, posteroventral rugosity; sp, stapedial pit; st.pr, suprastapedial process; tr, tympanic rim. Scale bars equal 1 cm.

refer to as the posteroventral rugosity, and is the incipient expression of the so-called posteroventral ascending rim (Bell, 1997) Note that the pterygoid process (pt.pr) in Figure 8 is one of the structures previously referred to as the "infrastapedial process" by Bell (1997). Additionally, the posteroventral rugosity (pvr) in Figure 8, in its most derived condition, is expressed as a thickened "posteroventral ascending rim" that contacts or nearly contacts the suprastapedial process as in *Selmasaurus* and *Ectenosaurus,* and has also been referred to as the "infrastapedial process" (Wright and Shannon, 1988; see also Palci et al., 2020, for alternate nomenclature).

There is a cluster of one large and four smaller foramina medially located and bounded ventrally by the articular border as in *Tethysaurus* and *Russellosaurus,* but not in later diverging Plioplatecarpines in which the area is covered with numerous small foramina. Lateral to these foramina is a rugose area extending laterally, the more medial portion of which is marked by dorsomedially trending striae which extend to the ventral margin of the gap between the incipient posteroventral ascending process and the more medially placed infrastapedial process. The area dorsal to this gap is the preserved portion of the alar bowl.

In lateral view, the preserved portion of the quadrate of *Sarabosaurus dahli* gen. et sp. nov. is rostrocaudally thin, similar to *Tethysaurus,* and the thick alar rim rises at a low angle anterodorsally. The comparable part of the quadrate is rostrocaudally thicker in *Russellosaurus*, and the alar rim originates in a relatively lower position, forming a larger radius of the alar rim, a trend that continues in later diverging plioplatecarpines.

In ventral view, the articular surface is bipartite, divided into a strongly convex medial part, the lateral portion of which rises and wraps around the ventrolateral side of the quadrate, visible in lateral view nearly half the distance to the insipient posteroventral ascending rim. This lateral part is offset from the medial part by a shallow oblique sulcus in ventral view. The medial part is damaged by a break in the posterior surface, but it is elongate as in *Tethysaurus*, composing about one third of the ventral surface, and is less convex and significantly narrower than the lateral part. In anterior view, the medial part bears a shallow sulcus formed by the anteriorly bending medial margin. The dorsolateral part rises anterodorsally, paralleling the alar recess.

Because most later diverging mosasaurids have well developed posteroventral ascending rims that at times approach and meet the infrastapedial process, Russell (1967) conflated the two structures, referring to them collectively as the "infrastapedial" process. However, we now know the structures have separate evolutionary paths. In *Russellosaurus* the incipient posteroventral ascending rim is expressed as a nearly circular rugosity suggesting ligamentous attachment. The posteroventral ascending rim is highly developed in later diverging forms such as *Plesioplatecarpus planifrons* and other taxa in the *Platecarpus*/*Plioplatecarpus* species group, in which it is relatively thin. In *Selmasaurus and Angolasaurus,* it is quite thick and meets the suprastapedial process. Both the minimally developed pterygoid process (pt.pr) and the posteroventral ascending rim condition in *Sarabosaurus dahli* gen. et sp. nov. are similar to the condition in *Tethysaurus*.

4.13. Mandibles

Both mandibles are present, but fragmentary (Fig. 9A–X). The dentaries are represented by numerous fragments (Fig. 9A–F, L–N), posterior mandible by a portion of the left articular-surangular (Fig. 9G–K), and parts of both splenials and a left angular fragment (Fig. 9O–X).

4.14. Dentary

The anterior part of the right dentary is preserved. It is robustly built and preserves four alveoli and remnants of a fifth. In lateral view, a small bulge extends in front of the first tooth position, comparable to the condition in the premaxilla and only slightly more than seen in *Russellosaurus.* In lateral view, the tooth bases are prominently visible above the dorsal margin. Slightly below mid-height, a row of four foramina is visible; the posterior three approximately ventral to tooth positions two, three, and four, and the anterior one ventral to the gap between the first and second tooth positions. A fifth foramen is visible on the ventrolateral face of the dentary approximately below the gap between the second and third tooth positions.

The medial ridge is low and the tooth roots broadly exposed (Fig. 9B, E). The roots are highly vascularized with prominent foramina at the bases on some of the tooth positions. Meckel's groove faces medially, about equally dividing the anteromedial face of the dentary, judging from the preserved anterior portion at the fourth tooth position (Fig. 9L) and can be traced anteriorly, to terminate anteriorly below the first tooth position. In *Russellosaurus* and more later diverging plioplatecarpines, it extends to the anterior margin of alveolus.

The most anterior tooth is relatively small, with succeeding teeth progressively larger judging from the diameter of the crown at the preserved cementum-enamel junction (CEJ) and the width of the dentary in dorsal view. This condition is probably similar in *Russellosaurus* (Polcyn and Bell, 2005). In later diverging plioplatecarpines, the anterior teeth are roughly equal in size and diameter to succeeding ones, but do diminish in size posteriorly in the last several tooth positions. The first tooth position has a deep posteromedial replacement pit and a shallower one is visible on the second. The third tooth position is in advanced replacement, with remnants of what appears to be a new replacement tooth in early stages of ankylosis, but breakage precludes certainty. The fourth tooth position shows no evidence of resorption. Remnants of the anterior wall of the fifth alveolus are present on the posterior surface. Based on the fragmentary material and comparisons with the combined premaxilla-maxilla tooth count, we estimate a minimum of thirteen dentary tooth positions.

4.15. Surangular-Articular

In dorsal view, the glenoid is longer than wide and composed primarily of articular, the surangular only contributes to an anterodorsally sloping, elevated buttress, as in *Russellosaurus* (Polcyn and Bell, 2005). In dorsal view, anterodorsal to the glenoid, the surangular margin trends anteromedially, but to a lesser degree than in *Russellosaurus*. Anterolateral to the glenoid, high on the lateral face, the remnant of the posterior surangular foramen can be seen. The path of the lateral suture between the surangular and articular is unclear; however, portions of the surangular suggest it reaches the posterior glenoid. The articular-surangular suture is clearly visible in medial view, curving anteroventrally to nearly horizontal anteriorly, suggesting the articular and surangular contribute about equally to the medial face anterior to the glenoid, as in *Russellosaurus* (Polcyn and Bell, 2005) and later diverging plioplatecarpines.

In *Tethysaurus,* the glenoid is wider than long and the articular is restricted to about a third of the medial face anterior to the glenoid whereas the surangular forms a transverse, thin bony buttress in front of the glenoid before sloping abruptly ventral to form the posterior part of the mandibular fossa. The surangular forms a narrow dorsal ridge lateral to the fossa.

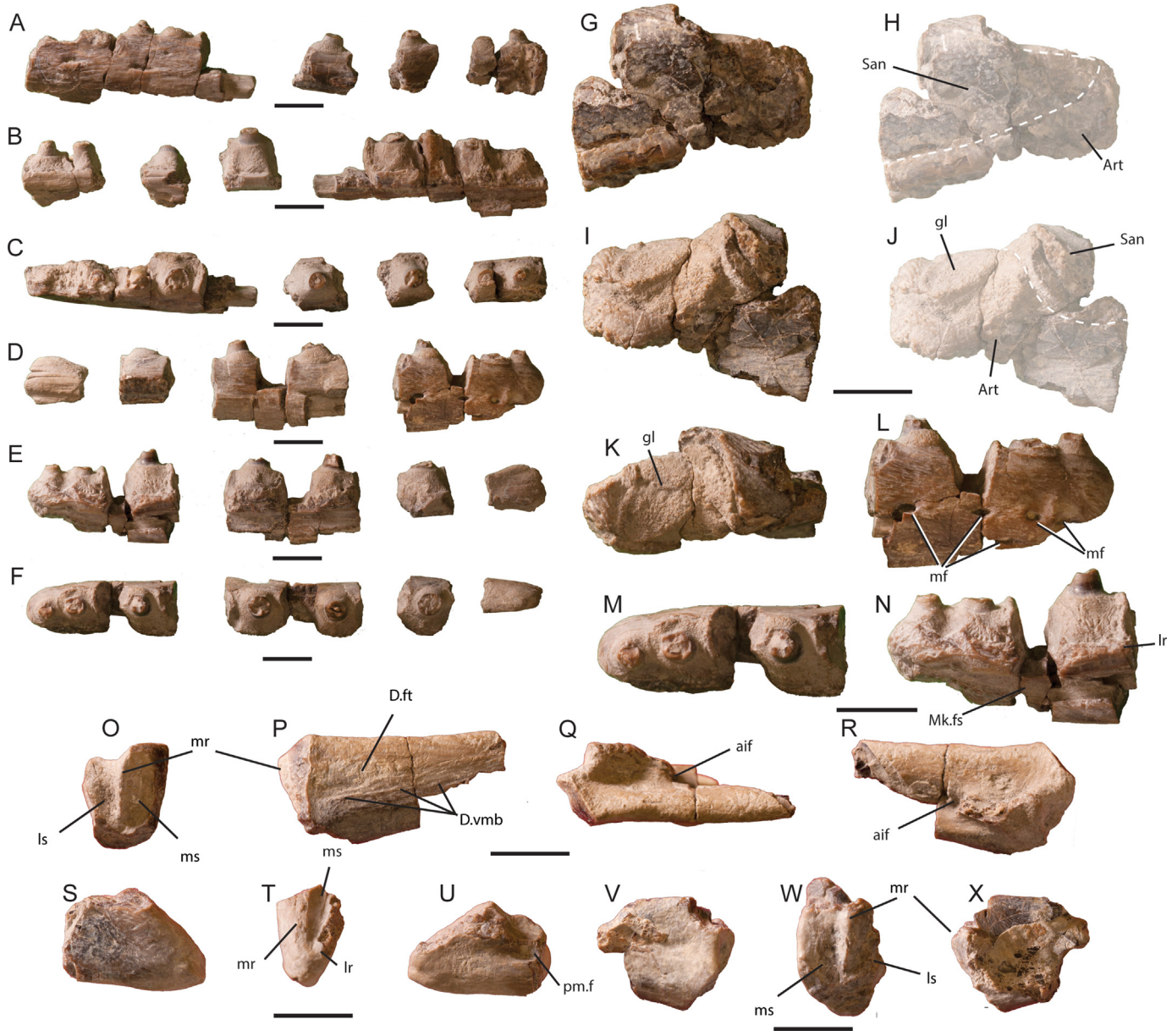

Fig. 9. Mandible elements of *Sarabosaurus dahli* gen. et sp. nov.. Left dentary in (A) lateral, (B) medial and (C) dorsal views. Right dentary in (D) lateral, (E) medial, and (F) dorsal views. Left surangular-articular fragment in (G, H) lateral, (I, J) medial, and (K) dorsal views. Anterior right dentary in (L) lateral, (M) dorsal, and (N) medial views. Portion of right splenial in (O) posterior, (P) lateral, (Q) dorsal, and (R) medial views. Anterior right angular fragment in (S) lateral, (T) anterior, and (U) medial views. Left splenial fragment in (V) lateral, (W) posterior, and (X) medial views. Abbreviations: aif, anterior inferior alveolar foramen; art, articular; d.ft, dentary facet; d.vmb, dentary posteroventral margin buttress; gl, glenoid; lr, lateral ridge; ls, lateral sulcus; mf, mental foramen (foramina); Mk.fs, Meckal's fossa; mr, medial ridge; ms, medial sulcus; pm.f, posterior mylohyoid foramen; san, surangular; spl, splenial. Scale bars equal 1 cm.

4.16. Splenial-Angular

The posterior ends of both splenials are preserved in part (Fig. 9O–R, V–X). In posterior view, the right preserves the medial margin and the left side of the dorsal margin. The left splenial preserves a portion of the lateral margin. The ventral margin is damaged on both. The anterior part of the left angular is preserved. On the posterior face of the splenial is a prominent narrow median ridge that extends ventrally three quarters of the vertical height of the surface (Fig. 9O, P). This median ridge and the surfaces lateral to it articulate with conjugate structures on the angular, forming the ventral part of the intramandibular joint.

The splenial-angular joint in mosasaurids has been described as a ball and socket joint (Rieppel and Zaher, 2000b). Although this description is generally true, in all mosasaurs, there is an additional descending ridge that originates at the posterodorsal-most part of the lateral dorsal margin and trends ventromedially to varying degrees amongst taxa. The ridge is widest dorsally and narrows ventrally. There is a corresponding notch on the dorsal part of the angular articular face that receives the ridge. In *Tethysaurus* and *Russellosaurus* the ridge is small and restricted to the dorsal part of the articulation. In *Platecarpus-Latoplatecarpus*, and *Plioplatecarpus*, the ridge is more pronounced, expanded dorsally and contributes to a high dorsolateral margin. The splenial-angular ridge of *Sarabosaurus dahli* gen. et sp. nov. is much more developed and more centrally positioned than in *Russellosaurus, Tethysaurus, Platecarpus, Latoplatecarpus*, and *Plioplatecarpus*, implying perhaps a high degree of immobilization or resistance to torsional loads. In

posterior view, the splenial is taller than wide and in lateral view has no distinct longitudinal facet for the dentary.

4.17. Axial Skeleton

The vertebral column is incomplete and fragmentary but all regions are represented. Counting only complete centra and isolated condyles, there are six cervical (including the atlas), twenty dorsal, one sacral, at least three pygal, and thirty-six caudal vertebrae.

4.18. Atlas

The atlas is represented by the odontoid (atlas centrum) and the body of the left atlas neural arch (Fig. 10A–H). The dorsal ramus of the atlas neural arch is missing. In lateral view, the preserved main body of the element is subtriangular, its base forming the lateral margin of the anterior articular face. The ventral margin is convex anteriorly and straight more posteriorly before meeting the base of the synapophysis. A small dorsal ridge rises from the synapophysis and slopes anteriorly before being truncated by the broken base of the missing dorsal ramus. The base of the anterior part of the dorsal ramus curves medially and is set back from the anterior face a very short distance at its narrowest point. It would have formed a small notch (char 91, Bell, 1997; Russell, 1967, pg.70) or embayment as seen in *Latoplatecarpus willistoni* (FHSM-VP16582), but not to the extent seen in *Ectenosaurus* and some mosasaurines (Russell, 1967). The anterior surface is approximately twice as tall as it is wide, and slightly pinched in the middle. In medial view outline is the mirror of the lateral view but has a thickened anteroventrally trending ridge running between the synapophysis and the anteroventral part of the bone. Other than a small amount of cortical bone visible on its dorsal margin, the anterior face, the medial face, and the posterior part of the synapophysis would have been covered with cartilage in life.

The odontoid is 1.6 times wider than tall, relatively wider than in later diverging plioplatecarpines. In dorsal view, the bone is pentagonal. The anterior facing portion has three sides, including a medial articulation for the basioccipital which is flanked by anterolaterally facing articulations for the atlas neural arches. The posterior margin, which articulates posteriorly with the axis centrum, is composed of two posterolaterally facing surfaces. There is a dorsal fossa whose anterior border approximates the curvature of the anterior margin in dorsal view and the posterior border forms an arc that is offset anteriorly from the posterior margin of the bone. In lateral view, the odontoid is wider at the top than at the bottom. The entire ventral surface of the odontoid is the articular facet for the dorsal part of the axis intercentrum.

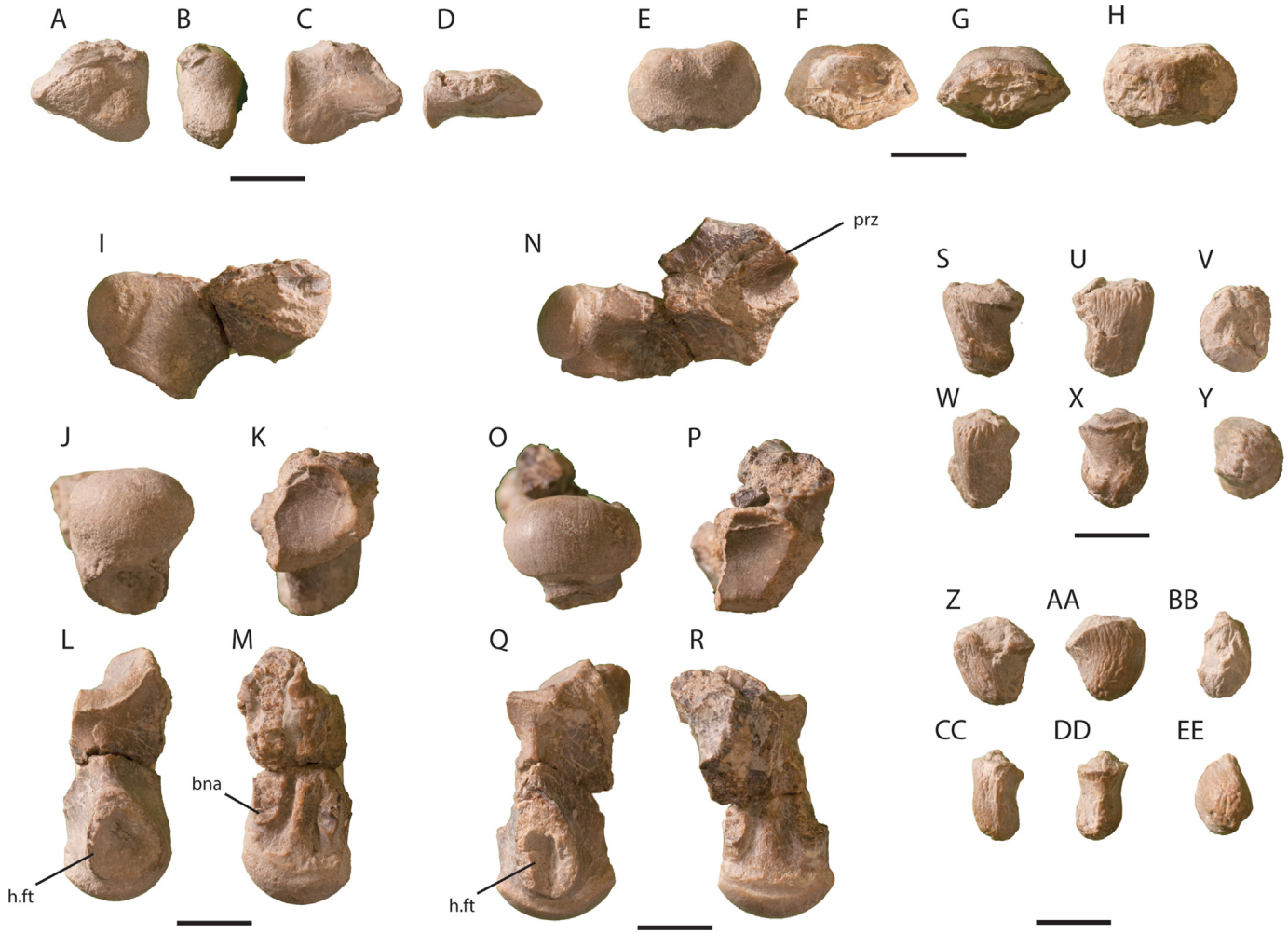

Fig. 10. Cervical vertebrae and associated elements of *Sarabosaurus dahli* gen. et sp. nov.. Left atlas neural arch in (A) medial, (B) anterior, (C) lateral, and (D) dorsal views. Odontoid in (E) anterior, (F) dorsal, (G) ventral, and (H) posterior views. Cervical vertebrae C4 and C5 in (I, N) left lateral (J, O) posterior, (K, P) anterior, (L, Q) ventral, and (M, R) dorsal views (lateral views reversed). Middle and posterior cervical hypophyses in (S, Z) left lateral, (U, AA) right lateral, (V, BB) dorsal, (W, CC) anterior, (X, DD) posterior, and (Y, EE) ventral views. Abbreviations: bna, base of neural arch; h.ft, hypophyseal facet; prz, prezygopophysis. Scale bars equal 1 cm.

4.19. Post-axis cervical vertebrae

Five hypopophysis bearing vertebrae, probably representing positions C3–C7, are partially preserved. The condyles in the cervical series are all broadly oval and dorsoventrally compressed, the anterior ones more so than the posterior (Fig. 10I–R). The pedicles for the hypopophyses are prominent and posteroventrally oriented. Their articular facets are subtriangular in shape, the apex of which points anteriorly to produce a rounded, pronounced central medial ridge that follows the anterior face of the hypopophysis and curves anteriorly to meet the ventral border of the cotyle. The bases of the synapophyses of C4 and C5 give rise anterodorsally to the prezygapophyses, its lateral face being a prominent narrow ridge. Another ridge of bone extends anteroventrally to the cotylar margin, and terminates dorsal to the ventral margin. The dorsal and ventral margins of the synapophyses converged posteriorly on the lateral surface and form a rounded ridge that meets the condyle in a dorsal position in lateral view. This ridge is more inflated and rounded on the more posterior cervicals. The depressed condyles of the cervical vertebrae are reminiscent of those in halisaurines, but are not reniform, its dorsal margin being convex as in *Tethysaurus* (Bardet et al., 2003).

Though all are missing, the broken bases of the neural arches indicate they would have run nearly the length of the dorsal surface, but exposing the centrum surface a small distance anterior to the condyles. Two hypapophyses from unknown positions are preserved (Fig. 10S–EE). They are somewhat crushed and asymmetrical, but would have likely been somewhat recurved rounded cones. There is some distal inflation in both that may reflect original morphology.

4.20. Trunk vertebrae

The first dorsal vertebra is represented only by the posterior portion. In ventral view, there is a protuberance at the midline, just anterior to the condylar margin, which is surrounded by highly vascularized bone that appears to be a hyperossification. This complex of structures is in a similar position as the pedicles in the

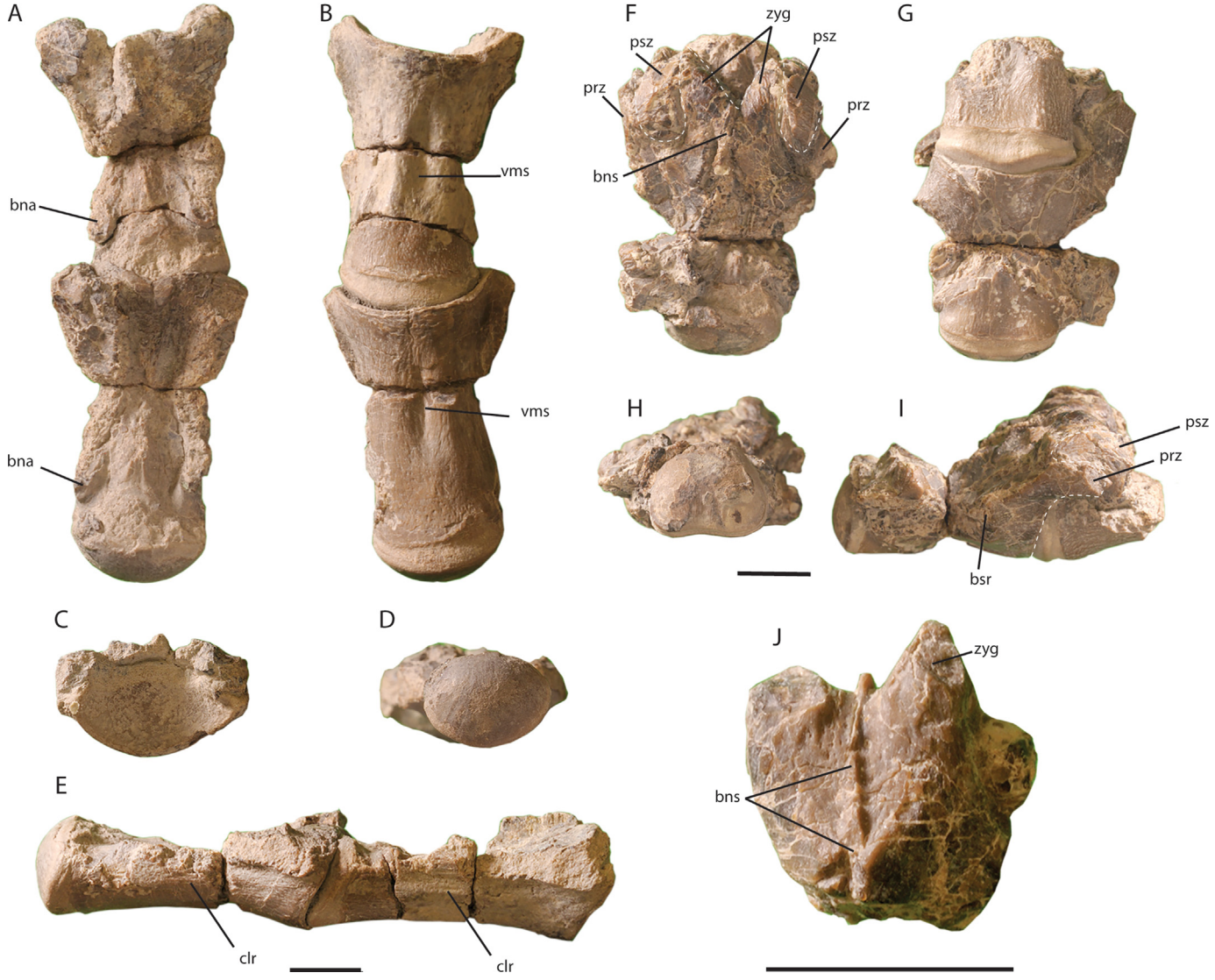

Fig. 11. Representative dorsal and sacral vertebrae. Mid-trunk vertebrae in (A) dorsal, (B) ventral, (C) anterior (D) posterior, and (E) right lateral views. Sacral and partial ?posterior trunk vertebrae in (F) dorsal, (G) ventral, (H) posterior) and (I) left lateral (reversed) views. Anterior neural arch fragment from unknown position in (J) dorsal view. Abbreviations: bna, base of neural arch; bns, base of neural spine; bsr, base of sacral rib; clr, centrum lateral ridge; prz, prezygopophysis; psz, postzygopophysis; vms, ventral median sulcus; zyg, zygosphene. Scale bars equal 1 cm.

preceding vertebrae, and is thus most likely an aberrant posterior expression of that developmental mechanism. The central protuberance bears two paramedian, small circular areas, rostrocaudally offset from one another by what appears to be ligamentous insertions. The condyle is broadly oval, with a small depression on its dorsal margin. In dorsal view, the anterior margin of the condylar tissue trends posteromedially in the first couple trunk vertebrae, but not in more posterior ones.

The most complete trunk vertebrae are longer than the cervicals (Fig. 11A–E). No synapophyses in the dorsal series are completely preserved, but based on the cross sections of the broken bases, they appear to originate near the cotylar border and posteriorly connect to a ridge that runs the lateral length to the condyle in a dorsal position in lateral view. Dorsally, some partial neural arches are preserved but badly crushed. They significantly overhang the cotyle and preceding vertebrae but no complete zygosphenes are preserved in place. The intercentral articulations are somewhat oblique, exposing the ventral part of the preceding condyle ventrally, but probably exaggerated by crushing. Ventrally, a median sulcus is visible approximate half the length of the centrum and offset anteriorly slightly. What are interpreted here as the last several dorsals, are relatively shorter than the preceding series. Postzygopophyses rise more vertically and medially than in more anterior trunk vertebrae.

4.21. Sacral vertebrae

A single relatively complete sacral vertebra is present (Fig. 11F–I). It is markedly shorter than the preceding trunk series. In dorsal view, the large zygosphenes are separated by a deep v-shaped anterior notch. Compared to the lower angle zygosphene articulations of the more anterior trunk series (Fig. 11J), the sacral zygapophenes have a high angle of articulation with zygantra on the medial part of the postzygapophyses of the preceding vertebra. The condyle is only slightly wider than tall. The broadest part is the ventral margin and is weakly convex medially. The sides slope dorsomedially, and the dorsal margin is slightly arched but flat in the center. The ventral surface is crushed, but appears to have been nearly flat with no ventral median sulcus. Long, thin prezygapophyses rise anterodorsally a short distance from the cotylar margin, about mid-centrum height. The sacral ribs are broken, but their bases suggest they were wide, nearly meeting the condylar margin posteriorly. Features of the sacral vertebra in *Sarabosaurus dahli* gen. et sp. nov. compare favorably with FHSM VP-17246, an isolated, but well-preserved sacral vertebrae from the Jetmore Chalk Member, of the Greenhorn Formation, near Salt Creek in southern Mitchell County, Kansas, USA (Everhart and Pearson, 2014; their Figure 4). The articular shape also compares well with the pygal figured in the description of *Tethysaurus* (Bardet et al., 2003, their Figure 2L). Both of which are also lower Turonian in age.

4.22. Pygal vertebrae

There are at least three non-chevron-bearing (pygal) caudal vertebrae. An anterior pygal is badly crushed but preserves the postzygapophyses well anterior to the condyle, suggesting the elongate prezygapophyses seen in the sacral series continue at least into the base of the tail (Fig. 12A–C). The centra of the pygals are approximately the length of the sacral vertebra. The broken bases of transverse processes are visible near the ventrolateral margin. They are thin and broad, occupying the length of the centrum, leaving only a small gap between posterior terminus of the base and condyle. The articular surfaces are comparable to, but not as relatively tall as the sacral, possibly due to crushing.

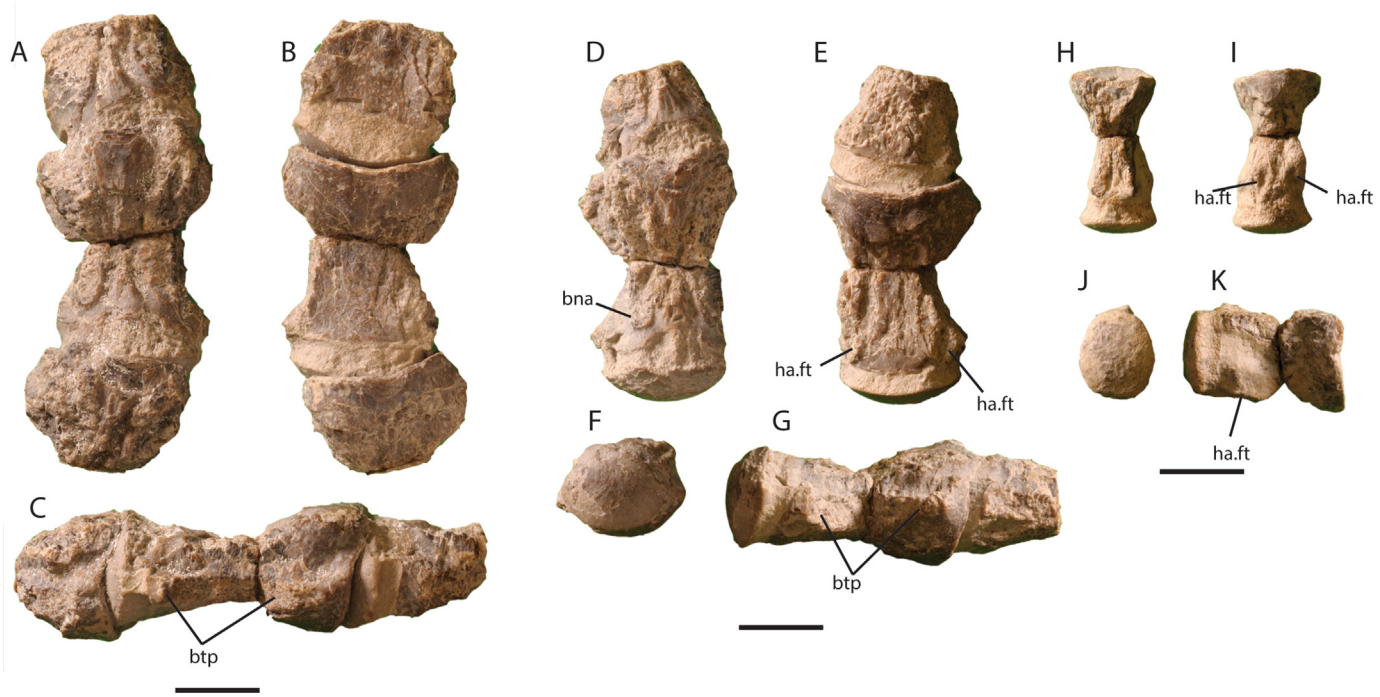

Fig. 12. Caudal vertebrae. Pygal vertebrae of *Sarabosaurus dahli* gen. et sp. nov. in (A) dorsal, (B) ventral, and (C) lateral views. Anterior to mid-caudal vertebrae in (D) dorsal, (E) ventral, (F) posterior, and (G) lateral views. Posterior caudal vertebra in (H) dorsal, (I) ventral, (J) posterior, and (K) lateral views. Lateral views reversed in C and G. Abbreviations: bna, base neural arch; btp, base of transverse process; ha.ft, hemal arch facet. Scale bars equals 1 cm.

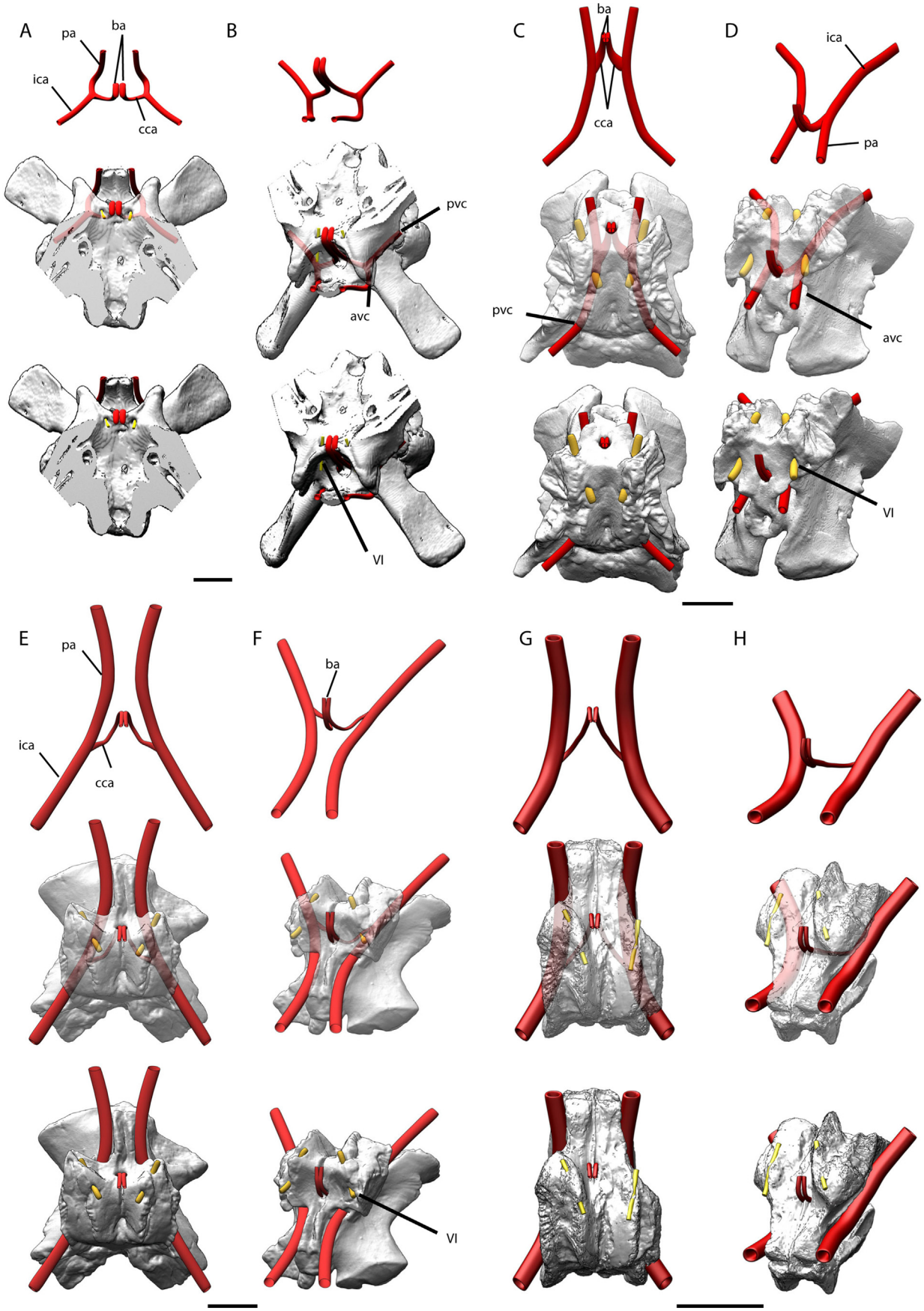
A
pa
ba
ica
cca
B
pvc
avc
VI
C
ba
cca
pvc
D
ica
pa
avc
VI
E
pa
ica
cca
F
ba
VI
G
H

4.23. Post-pygal caudal vertebrae

The caudals are all relatively long compared to later diverging mosasaurs (Fig. 12D–K), but similar to those seen in *Tethysaurus* (Bardet et al., 2003). The domed articular surfaces are broadly oval in posterior view, but almost as tall as wide, and appear to articulate vertically in lateral view. Posteriorly, the articulating surface of vertebrae are slightly taller than wide. In ventral view, facets for hemal arches are present. They are relatively small and low, at about the level of the ventral surface but in a far posterolateral position, their lateral extent exceeds the width of the condyle.

5. Vascularization of the Basisphenoid in Mosasaurids

Most mosasaurids, retain the plesiomorphic carotid circulation pattern (Figs.13A–H). Arguably, the most remarkable aspect of *Sarabosaurus dahli* gen. et sp. nov. is the presence of a novel basicranial circulation pattern, preserved in the basisphenoid fragment (Fig. 14A–I), and shared only with plioplatecarpine mosasaurids. The incipient expression of this condition is seen in *Tethysaurus* (Fig. 14J, K), while better known late diverging plioplatecarpines display extreme development of this character complex (Fig. 14L, M). To further document this evolutionary novelty, we briefly describe the basicranial vascularization across Mosasauridae, recognizing three distinct patterns referred to hereafter as Type 1, Type 2, and Type 3.

5.1. Type 1

The plesiomorphic squamate pattern is exemplified by *Varanus* (Fig. 13A, B), in which the internal carotid artery branches within the vidian canal, giving rise to the cerebral carotid artery, which emerges within the posterior part of the sellae turcica and gives rise to the basilar artery. There are no accessory anterolateral foramina nor an internal canal in the basisphenoid (98:0; 99:0) or basioccipital (100:0). This condition is retained in the mosasaurid subfamilies Halisaurinae, Mosasaurinae, and Tylosaurinae (Fig. 13C–H), but unknown in dolichosaurids and other basal branching mosasaurids (e.g., *Aigialosaurus*). In all cases, the cerebral carotid canal is significantly smaller than the vidian canal. In halisaurines, the posterior vidian canal enters the basisphenoid at the posterior suture with the basioccipital, and in some taxa leaves a shallow sulcus on that element (Polcyn et al., 2012; Fig. 13C, D). In lateral view, the posterior vidian canal cannot be seen in halisaurines and the path of the internal carotid is deep, the lateral wall of the vidian canal thick. In all other mosasaurids the posterior opening of the vidian canal is well anterior to the basisphenoid-basioccipital suture. The canal takes a shallow path, its lateral wall composed of a thin sheet of bone which is often damaged, exposing the vidian canal laterally. In all mosasaurids, the anterior opening of the vidian canal is dorsal to the base of the basipterygoid processes.

5.2. Type 2

This pattern is exemplified by *Tethysaurus* (Figs.14J, K and 15A-H), in which *de novo* canals enter the basisphenoid anterolaterally, trend posteromedially and converge to exit via a foramen high on the posterior wall of the sella turcica, apparently supplanting the so-called basilar artery (sensu Russell, 1967; ch98:1). This canal is visible dorsal to the vidian canal, which carries the internal carotid (Fig. 15A–E), the two anteriorly separated by a ridge of bone on the lateral wall of the sella turcica, which posteriorly manifests as a septum. Rieppel and Zaher (2000a; citing G. L. Bell, personal communication) noted a subdivision of the anterior part of the vidian canal is present in many plioplatecarpine taxa and may be a synapomorphy of that subfamily. We confirm that observation though it is somewhat diminished in taxa such as *Platecarpus* compared to the condition in *Tethysaurus* (e.g., Figs. 15D, E, L and 16D, F, K, L). Once they enter the basisphenoid, the canals converge medially and exit via a large foramen high on the posterior wall of the sella turcica, just below the dorsum sellae as the basilar artery. There is no posterior extension of the canals into the body of the basisphenoid as seen in later diverging plioplatecarpines (Figs. 14L, M, 15I–L, 16A–C; ch99:0). Given the similar position of the foramen, it does appear to supplant the function of the basilar artery seen in the Type 1 pattern, but the relatively large diameter compared with non-plioplatecarpine mosasaurs suggests increased carrying capacity. In addition to the *de novo* canals for the basilar artery noted above, in *Tethysaurus*, the cerebral carotid branches from the internal carotid within the vidian canal at about the rostrocaudal level of the dorsum sellae and emerges near the center of the sella turcica (Fig. 15E) as paired foramina separated by a thin median ridge.

Russellosaurus also appears to possess the Type 2 pattern (Fig. 16D, E; ch98:1, ch99:0). The anterior part of the vidian canal is divided into dorsal and ventral canals by a lateral ridge, and a large diameter foramen is present on high on the posterior wall of the dorsum sellae, but higher than in *Tethysaurus*, its posterior wall reaching the dorsal surface of the basisphenoid as in *Sarabosaurus dahli* n. gen. et sp. nov.. However, the basisphenoid in the holotype and only specimen of *Russellosaurus* preserving the braincase, is crushed and broken in such a way to preclude accurately tracing connectivity of the internal paths of the canals in CT data, and thus many details are unknown. Nonetheless, in addition to the bifurcated anterior canal and large foramen high on the posterior wall of the sella turcica, *Russellosaurus* shares with *Tethysaurus*, a rostrocaudally short and tall sella turcica, bounded by well developed, thin crista trabeculae, which meet the clinoid processes dorsally, and at the convergence of those structures, is the anterior exit for the abducens nerve (Fig. 15E). Both *Tethysaurus* and *Russellosaurus* show foramina entering the basioccipital floor, but in both cases, those vessels can be traced to exit the ventral surface of that element and do not pass into the basisphenoid (100:0).

5.3. Type 3

This pattern is present in all late diverging plioplatecarpines (sensu Konishi and Caldwell, 2011) such as *Latoplatecarpus* and *Plioplatecarpus* (Fig. 16F, G and H-L respectively; ch98:1, ch99:1, ch100:1), but is shown here to also be present in *Sarabosaurus dahli* n. gen. et sp. nov. (Figs. 7A–E, and 14A–I) and *Yaguarasaurus* (Fig. 16A–C). In this condition, the anterior origin of the basilar artery is similar to that described for *Tethysaurus* above; however, the sella turcica is typically narrower and more drawn out in these forms and the lateral ridge more subtly expressed. As described by Russell (1967), the basilar artery enters the anterolateral basisphenoid, dorsal to the internal carotid artery, and near the

Fig. 13. Braincase comparisons. *Varanus komodensis* partial braincase (A, B), *Halisaurus arambourgi* NHMM-LV-2005-1A (C, D), *Clidastes propython* YPM1368 (E, F), and *Tylosaurus proriger* (G, H) in dorsal and anterodorsolateral oblique views respectively with isolated internal carotid and branches, semi-transparent, and opaque renderings of the bone from top to bottom for each taxon. Abbreviations: alc.dna, anterolateral canal for the de novo artery; av.dna, anterior vestibule de novo artery; avc, anterior vidian canal; ba, basalar artery; bo.ft, basioccipital facet; cca, cerebral carotid artery; dna, de novo artery; ica, internal carotid artery; lhv, lateral head vein; pa, palatine artery; pcc, posterio cerebral carotid artery; pro.ft, prootic facet; pvc, posterior vidian canal; sta, sella turcica artery; VI, abducens nerve. Scale bars equal 1 cm for A- F and 5 cm for G and H.

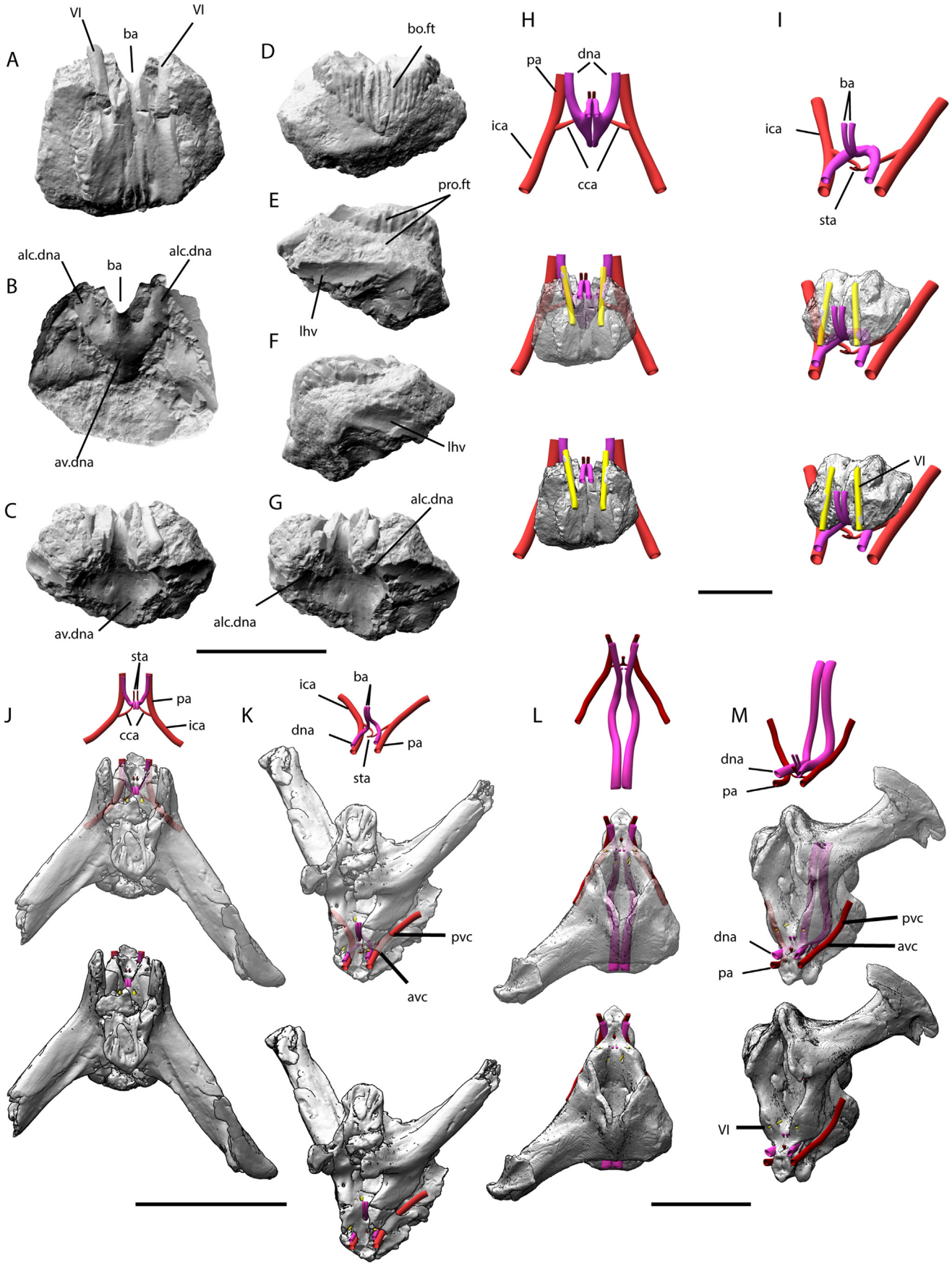
A
VI
ba
VI
B
alc.dna
ba
alc.dna
av.dna
C
av.dna
D
bo.ft
E
pro.ft
lhv
F
lhv
G
alc.dna
alc.dna
H
pa
dna
ica
cca
I
ba
ica
sta
VI
J
sta
pa
cca
ica
K
ica
ba
dna
pa
sta
pvc
avc
L
M
dna
pa
pvc
dna
avc
pa
VI

posterior part of the sella turcica. Once it enters the basisphenoid, this canal trends posteromedially, in some cases giving rise to a branch emerging below the dorsum sellae as one or two small foramina reminiscent of the basilar artery in Type 1 in terms of size and position, while the canal continues posterior as a vestibule or canal(s) within the posterior part of the basisphenoid. The path crosses into the basioccipital as paired canals or a single bilobate canal, and emerges on the posterior part of the dorsal surface of the basioccipital as paired foramina or a single bilobate foramen.

Although we have continued the usage of the term basilar artery for the artery that rises just below the dorsum sellae from the paired *de novo* structures described above in mosasaurs in both the Type 2 and Type 3 conditions, though likely analogous in function, it is not homologous with that in other lepidosaurs. In the Type 1 condition, the basilar artery rises from the paired cerebral carotid in the posterior sella turcica and continues posteriorly into the medullary cavity, merging as a single median vessel (Rahmat and Gilland, 2014; Kier et al., 2022).

5.4. Functional implications

The acquisition and elaboration of the unique basicranial circulation patterns in plioplatecarpine mosasaurids warrants brief exploration of functional implications. In the Type 2 condition, there is no connection between the internal vascularization of the basisphenoid and that of the basioccipital. The foramina on the floor of the basioccipital in the most basal branching forms are small, paired, and communicate with small ventral foramina of that element. The foramen just below the dorsum sellae is relatively large, comparable to that in the Type 1 condition. In the Type 3 condition, the foramina on the floor of the basioccipital increase in size in later diverging taxa, and coalesce to form a single bilobate foramen in some taxa. In many taxa the dorsal foramen communicates with a single or multiple small foramina on the ventral basioccipital, the main trunk continuing anteriorly, crossing the basioccipital-basisphenoid articulation, and uniting with the basisphenoid de novo vascularization. In these forms, the foramen just below the dorsum sellae is typically smaller than in either the Type 1 or Type 2 conditions, suggesting a lower carrying capacity of the vessel it transmits. Judging by the morphology of the foramina (or foramen) on the floor of the basioccipital, the trajectory of the posterior vessels exits in a posterodorsal direction, at a very low angle, forming shallow sulci, and strongly suggesting they continue posteriorly to exit the ventral foramen magnum. We suggest here that this is likely evidence of a connection with the thoraco-vertebral arteries. This condition is extremely rare among squamates, but documented in several arboreal snakes, possibly an adaptation to counter disruption of blood supply due to the effects of gravity while climbing (Zippel et al., 1998 and references therein).

The relatively small diameter of the canal branching from the internal carotid and carrying the cerebral carotid to the sella turcica in plioplatecarpines, which we refer to as the sella turcica artery (sta; Fig. 14J–M), suggests that it does not significantly contribute to the anterior cerebral blood supply. Instead, the large cross-sectional area of the canals through the basicranium in the Type 3 condition significantly exceeds the cross-sectional areas of the vidian canals, suggesting the majority of the blood supply to the brain in late diverging plioplatecarpines is via thoraco-vertebral arteries with reduced reliance on the internal carotid arteries. Given the vascular arrangement of the ventral brain in lepidosaurs (Rahmat and Gilland, 2014; Kier et al., 2022), it is likely that this posterior source bifurcated, sending one branch though the internal path (evidenced by the foramina) and a second along the floor of the medullary cavity, functionally supplanting the basilar artery.

In vertebrates generally, the blood supply to the brain is primarily via the internal carotid arteries, though exceptions occur (Rahmat and Gilland, 2014). In mammals generally, the carotid blood supply is augmented to the hindbrain, to varying degrees, by connections with the vertebral blood supply (Rahmat and Gilland, 2014). In cetaceans, cerebral circulation is highly modified, the majority of the blood supply coming from a thoraco-spinal retia associated with the meningeal and intercostal arteries and not the carotid, vertebral, or occipital arteries (Viamonte et al., 1968; see also Blix et al., 2013, and references therein) and intracranially supplying a complex anastomosing network of vessels. Development of this circulation pattern has been interpreted as a means of dampening arterial pressure pulses (Vogl and Fisher, 1982; Lillie et al., 2022), protecting the brain against damage during diving (Dormer et al., 1977), and as a means of diffusing nitrogen into the thoracic fat which is vascularized by the rete thus avoiding decompression sickness (Blix et al., 2013). Though highly speculative, these interpretations may also extend to plioplatecarpine mosasaurids; however, we are severely limited by lack of preservation of soft tissue. Nonetheless, the onset and evolution of this morphological complex in plioplatecarpine mosasaurs does suggest a shift in cerebral blood supply from predominantly carotid to predominantly thoraco-vertebral. Additionally, the trend toward increased carrying capacity of the de novo canal through the basicranium through time suggests that selective forces, irrespective of specific functional advantage, played a large role in the evolution of plioplatecarpine mosasaurids.

6. Phylogenetic analysis

As shown above, the basicranial circulation pattern present in *Sarabosaurus dahli* gen. et sp. nov., a pattern unique among Squamata, is shared only with Plioplatecarpinae (sensu Konishi and Caldwell, 2011) and some Turonian taxa that have been previously recognized as basal branching, non-tylosaurine russellosaurians (e.g., Polcyn and Bell, 2005; Konishi and Caldwell, 2011; Palci et al., 2013). Furthermore, previous phylogenetic analyses have recovered tylosaurines nested within the clade Russellosaurina, defined by Madzia and Cua (2017) to “contain the species *R. coheni*, *Y. columbianus*, *T. nopcsai*, the clade Plioplatecarpinae, and the clade Tylosaurinae” and citing inferences of Bell and Polcyn (2005), Dutchak and Caldwell (2006), and Cuthbertson et al. (2007). Therefore, to ascertain the effect of these new data on prior hypotheses of the interrelationships of russellosaurian mosasaurs, we performed a preliminary phylogenetic analysis using the character taxon matrix of Konishi and Caldwell (2011) with corrections and additions noted in the supplementary material. This matrix was selected because of its focus on plioplatecarpine ingroup relationships, but more importantly, its inclusion of

Fig. 14. Braincase comparisons continued - *Sarabosaurus dahli* gen. et sp. nov.. Partial basisphenoid in (A) dorsal, (B) ventral, (C) anterior, (D) posterior, (E) left lateral, (f) right lateral, and (G) anteroventral oblique views. Reconstructed vascularization in (H) dorsal and (I) anterodorsolateral oblique views showing isolated internal carotid and branches and de novo artery, with semi-transparent, and opaque renderings of the bone from top to bottom. *Tethysaurus nopscai* (GM1) in (J) dorsal and (K) anterodorsolateral oblique views. *Plioplatecarpus peckensis* (MOR1062) in (L) dorsal and (M) anterodorsolateral oblique views. (G, H) in dorsal and anterodorsolateral oblique views respectively. Anatomical abbreviations: alc.dna, anterolateral canal for the de novo artery; av.dna, anterior vestibule de novo artery; avc, anterior vidian canal; ba, osteri artery; cca, cerebral carotid artery; dna, de novo artery; ica, internal carotid artery; lhv, lateral head vein; pa, palatine artery; pcc, osterior cerebral carotid artery; pvc, posterior vidian canal; sta, sella turcica artery. VI, abducens nerve. Scale bars equal 1 cm for A- I and 5 cm for J-M.

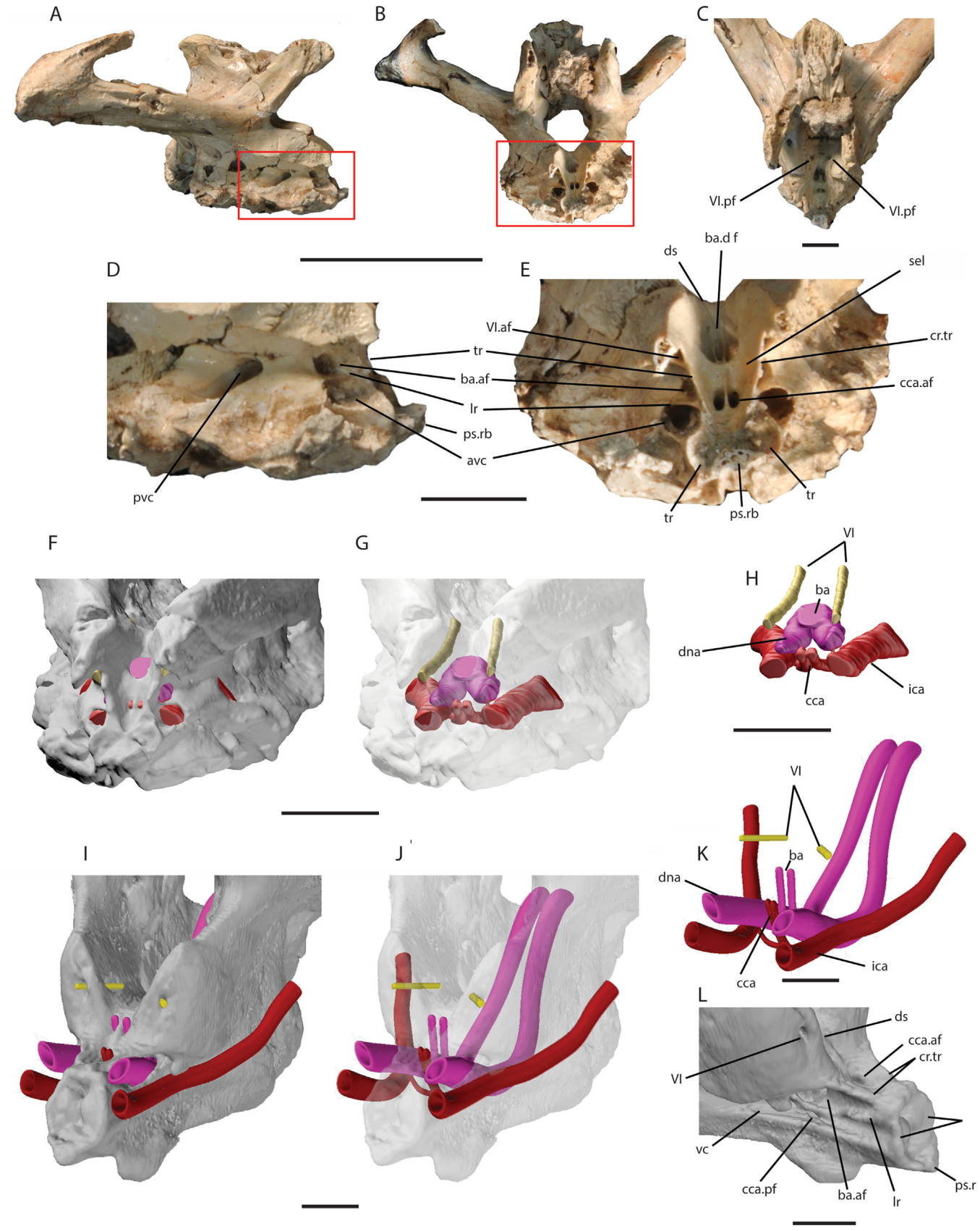
A
B
C
Vl.pf
Vl.pf
D
pvc
tr
ba.af
lr
ps.rb
avc
E
ba.d f
ds
sel
Vl.af
cr.tr
cca.af
tr
ps.rb
tr
F
G
H
Vl
ba
dna
ica
cca
I
J
K
Vl
ba
dna
ica
cca
L
ds
cca.af
cr.tr
Vl
vc
cca.pf
ba.af
lr
ps.r

tylosaurines and other taxa previously recognized as basal branching russellosaurians (sensu Madzia and Cua, 2017). We use the entire ingroup taxon selection of Konishi and Caldwell (2011) to which we add *Sarabosaurus dahli* gen. et sp. nov.. We did not add taxa such as *Romeosaurus* (Palci et al., 2013) and *Pannoniasaurus* (Makadi et al., 2012) that have previously been recognized as basal branching russellosaurians, because they do not preserve braincase anatomy and thus do not allow verification of basicranial vascularization patterns.

The analysis was performed in PAUP Version 4.0a (Swofford, 2002) using the branch and bound algorithm with all characters unordered and of equal weight, gaps were treated as missing data, multistate treated as uncertainty, the addition sequence set to furthest, and zero length branches set to collapse as polytomies. *Clidastes propython* and *Kourisodon puntledgensis* were used as a monophyletic outgroup. The apomorphy list was interpreted using the delayed transformation (DELTRAN) setting. Bootstrap values were generated in PAUP using heuristic search with 1000 replicates and 100 characters resampled in each replicate. Bremer indices were computed in PAUP with scripts generated in TreeRot V.3 (Sorenson and Franzosa, 2007) based on the recovered consensus tree.

The analysis yielded 9 equally parsimonious trees of 245 steps, with 86 of the 100 characters being parsimony-informative, and with a consistency index (CI) of 0.7224, CI excluding uninformative characters is 0.7043, the retention index (RI) is 0.7778, and the rescaled consistency index (RC) is 0.5619. The strict consensus and bootstrap trees are shown in Figure 17A annotated with Bremer and bootstrap values. The strict consensus of the 9 most parsimonious trees recovers the 4 Turonian taxa in a monophyletic clade, which forms a polytomy with *Ectenosaurus* and the clade containing the later diverging plioplatecarpines, to the exclusion of the tylosaurines. The bootstrap analysis additionally collapses *Angolasaurus* and *Selmasaurus* into the aforementioned polytomy. Bremer support for the clade composed of the Turonian taxa is relatively poor as are the bootstrap values, but there is good support for the *Platecarpus, Latoplatecarpus, Plioplatecarpus* clade. There is also strong Bremer and bootstrap support for a monophyletic Tylosaurinae.

Interestingly, the clade containing the 4 Turonian taxa, recovered in both the strict consensus and bootstrap trees, displays a retrograde evolutionary pattern, with relatively plesiomorphic forms such as *Tethysaurus and Russellosaurus* in the most derived position and *Yaguarasaurus* at its base. With respect to the basicranial circulation pattern, the recovered topology suggests the most derived expression (Type 3) evolves first with a reversal to Type 2 in the otherwise plesiomorphic and older forms (*Russellosaurus*, and *Tethysaurus*). Examination of character state distributions suggests the recovered topology is likely the result of implicit polarization of unordered characters, relative to the late diverging mosasaurine outgroup and included tylosaurines. Thus, to test the effect of taxon selection on ingroup tree topology, we performed a second analysis using the same settings and parameters as the first analysis, but restricting the ingroup to the more inclusive Plioplatecarpinae and deleting the mosasaurines and tylosaurines. For this second analysis, we use a varanoid outgroup following the recent phylogenetic analysis of Mosasauria by Augusta et al. (2022), in which mosasaurians (mosasauroids plus dolichosaurids) were recovered as the sister taxon to Varanoidea within Anguimorpha.

The second analysis recovered 3 equally parsimonious trees of length 187 with a consistency index (CI) of 0.7807, CI excluding uninformative characters is 0.7602, the retention index (RI) is 0.8194, and the rescaled consistency index (RC) is 0.6397, on the basis of 73 parsimony-informative characters. The consensus and bootstrap trees are illustrated in Figure 17B annotated with Bremer indices and bootstrap values. As in the first analysis, the Bremer indices show strong support for the relationships of the better-known post-Turonian plioplatecarpine taxa, but less so among the more basal branching Turonian taxa, also reflected in the bootstrap support (Fig. 17B).

7. Discussion

7.1. Phylogenetic patterns

Our phylogenetic analysis, using the character-taxon matrix and methods of Konishi and Caldwell (2011) and the modifications noted above, recovered a monophyletic clade comprised of *Tethysaurus, Russellosaurus, Sarabosaurus*, and *Yaguarasaurus* and taxa previously referred to Plioplatecarpinae (sensu Konishi and Caldwell, 2011), to the exclusion of Tylosaurinae. Though not surprising, it is significant in that numerous prior analyses consistently recovered a monophyletic tylosaurine clade nested between the basal branching Turonian russellosaurian taxa and the better-known post-Turonian plioplatecarpine taxa (Polcyn and Bell, 2005; Caldwell and Palci, 2007; Konishi and Caldwell, 2011; Makadi et al., 2012; Palci et al., 2013). Nonetheless, there remains uncertainty regarding basal branching patterns of the more inclusive Plioplatecarpinae as defined here, depending on outgroup selection and taxon inclusion. In our first analysis above, the Turonian taxa (*Tethysaurus, Russellosaurus, Saraboiosaurus*, and *Yaguarasaurus*) are united in a basal branching clade that is the sister taxon to the advanced plioplatecarpines, but that clade exhibits a counter-intuitive pattern of retrograde evolution. Alternatively, as shown in our second, more restrictive analysis, *Sarabosaurus dahli* gen. et sp. nov. is recovered as the sister taxon of *Yaguarasaurus* plus all other Plioplatecarpines and *Russellosaurus* and *Tethysaurus* as successive, more basal branching sister taxa to *Sarabosaurus dahli* gen. et sp. nov.. The branching pattern of the Turonian taxa in the second analysis is more consistent with their stratigraphic occurrence. The lower Turonian *Tethysaurus* is nearly the oldest, and is the most plesiomorphic taxon within the ingroup and its basal position recovered – a position originally suggested by Bardet et al. (2003) – appears justified as does the position of *Yaguarasaurus*, given the advanced nature of its basicranial circulation (Type 3) and its late Turonian age. The relatively basal position of *Russellosaurus* also seems reasonable, sharing the Type 2 circulation pattern with *Tethysaurus*; however, in some respects *Sarabosaurus dahli* gen. et sp. nov. retains the more plesiomorphic condition of certain characters. For instance, the quadrate in *Sarabosaurus dahli* gen. et sp. nov. possesses a thick anteroventral part of the alar (tympanic) rim as in *Tethysaurus*, while that part of the alar rim in *Russellosaurus* is thin as seen in later diverging forms (compare Fig. 8). *Sarabosaurus dahli* gen. et sp. nov. is also more similar to *Tethysaurus* in the

Fig. 15. Braincase comparisons continued. *Tethysaurus nopscai* (MNHN GOU 2) in (A) right lateral, (B) anterior, and (C), anterodorsal views. Details of anterior basisphenoid in (D) right lateral and (E) anterior views. CT rendering of the anterior braincase of *Tethysaurus nopscai* (MNHN GOU 2) in left anterolateral oblique view with (F) opaque, (G) semi-transparent, and (H) transparent surface views. CT rendering of the anterior braincase of *Plioplatecarpus peckensis* (MOR 1062) in left anterolateral oblique view with (I) opaque, (J) semi-transparent, and (K) transparent surface views, and (L) Right anterolateral and slightly dorsal view of the anterior basisphenoid. Anatomical abbreviations: ba.af, anterior foramen for basilar artery; ba.c, basilar artery canal; ba.df, dorsal foramen for basilar artery; ba.pf, posterior foramen for basilar artery; cr.tr, crista trabelcula; ds, dorsum sellae; lhv, lateral head vein; lr, lateral ridge; m.f, magnum foramen; o.c, occipital condyle; ps.rb. parasphenoid rostrum base; sel, sella turcica; tr, trabecula; VI, abducens nerve; VI.af, anterior foramen for abducens nerve; VI.pf, posterior foramen for abducens nerve. Scale bars equal 10 cm for A and B, and 1 cm for C–L.

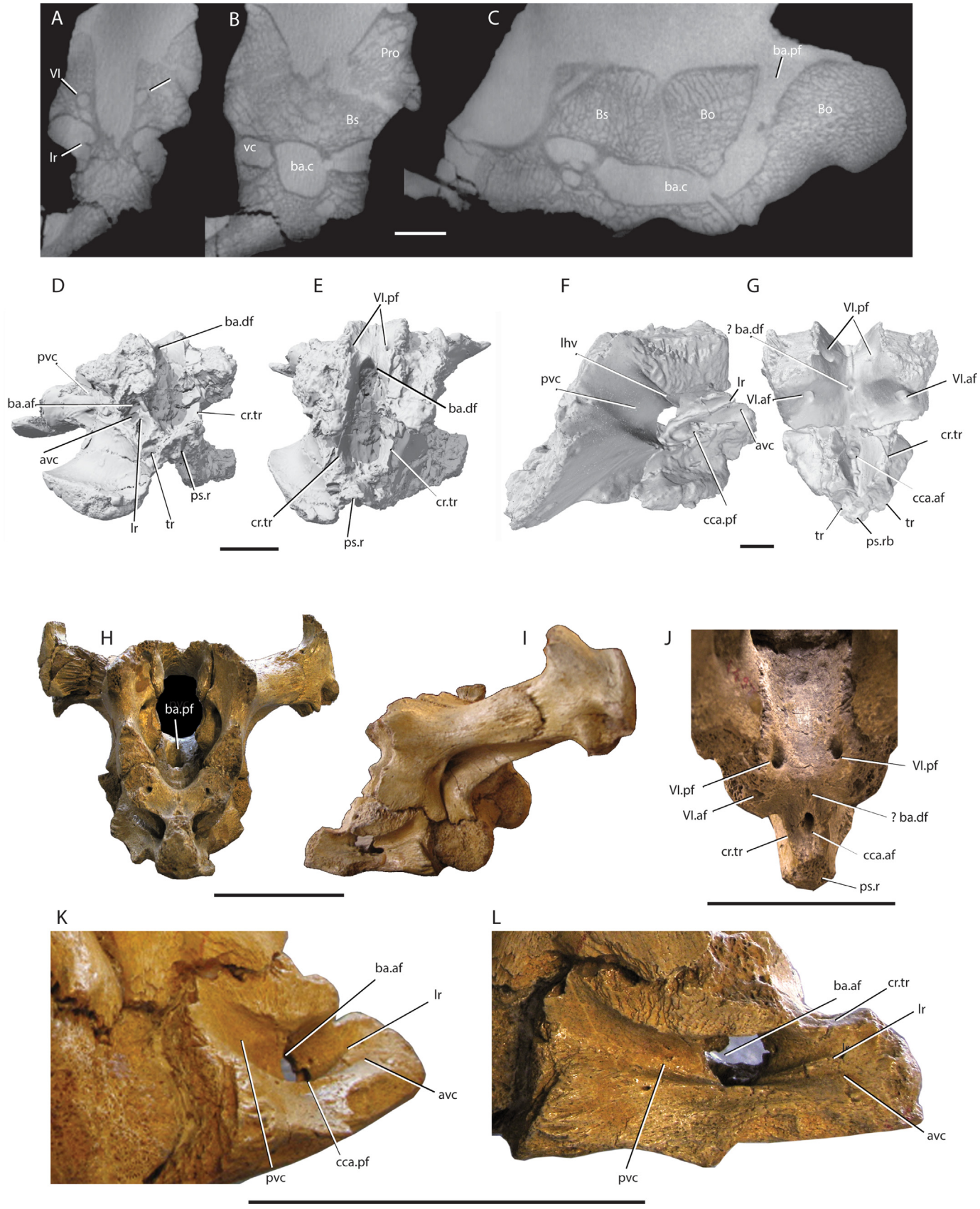

Fig. 16. Braincase comparisons continued. Select μCT slices of the braincase of *Yaguarasaurus columbianus* (BRV 68) transverse section positioned at (A) just anterior to cerebral carotid dorsal exit in sella turcica, (B) transverse section posterior to the basilar artery anterior foramen, and (C) sagittal section taken near the midline to show the path of basilar artery through the basicranium. Basisphenoid of *Russellosaurus coheni* (SMU73056) in (D) right anterolateral and slightly dorsal and, (E) anterodorsal views; *Latoplatecarpus willistoni* (SMU 77747) in (F) right posterolateral, (G) anterodorsal views. *Plioplatecarpus marshi* (IRSBN R38) in (H) anterior, (I) left lateral view, (J) detail of anterior braincase in anterodorsal view, (K) detail of anterior basisphenoid in posterolateral, and (L), lateral views. Anatomical abbreviations as in Fig. 15. Scale bars equal 1 cm for A–G and 10 cm for H–L.

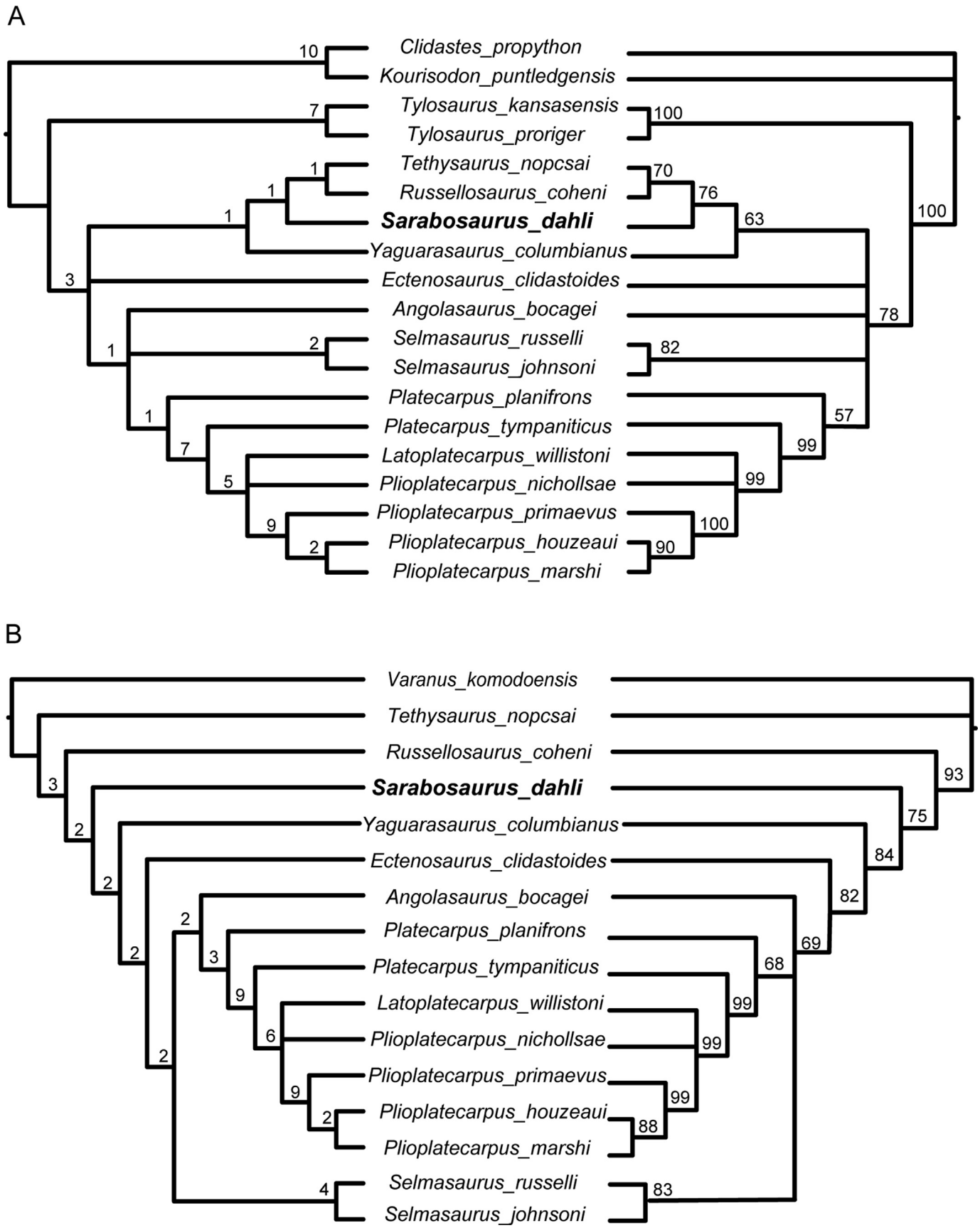

Fig. 17. The strict consensus (left) and bootstrap (right) trees annotated with Bremer indices and bootstrap values for two phylogenetic analyses. (A) Analysis using the complete character taxon matrix of Konishi and Caldwell (2011) plus the inclusion of *Sarabosaurus dahli* gen. et sp. nov.; and (B), a reduced taxon analysis using a varanoid outgroup. See text for details and discussion and supplementary materials for supporting data.

rostrocaudal thickness of the quadrate. The pterygoid in *Sarabosaurus dahli* gen. et sp. nov., though fragmentary, shares characters with *Tethysaurus,* such as high tooth count and the tooth row continuing onto the basisphenoid ramus, while in *Russellosaurus*, the tooth count is reduced, and the tooth row terminates anterior to the divergence of the pterygoid and basisphenoid rami. Finally, the dermal sculpting present on the frontal and maxillae of *Sarabosaurus dahli* gen. et sp. nov. appears to be primitive, given the lack of such features in *Russellosaurus*, *Yaguarasaurus* and the remainder of the more inclusive Plioplatecarpinae, but it is present on the dorsal surface of the frontal of at least some specimens of *Tethysaurus* (e.g., MNHN GOU 3; Bardet et al., 2003; their Figure 2A), exhibiting sculpting on posterior part of the dorsal surface of the frontal. In contrast to these apparently plesiomorphic characters retained in *Sarabosaurus dahli* gen. et sp. nov., it possesses the relatively derived basicranial circulation pattern (Type 3) as shown above.

7.2. Early radiations of major clades of mosasaurids

Irrespective of phylogenetic relationships among *Tethysaurus, Russellosaurus, Sarabosaurus*, and *Yaguarasaurus*, the temporal distribution and morphological disparity of these early forms, suggest rapid diversification of plioplatecarpines following an early Turonian cladogenesis. The timing of the origins of subfamily level clades was commented on by Polcyn et al. (2008; see also Polcyn et al., 2014), who suggested an early Turonian cladogenesis of Russellosaurina and early differentiation of plioplatecarpines, a concept further supported here. *Sarabosaurus dahli* gen. et sp. nov., as the oldest member of the clade coming from the upper part of the *Watinoceras devonense* Ammonite Zone, *Tethysaurus nopcsai* from the slightly younger *Mammites nodosoides* Ammonite Zone (Kennedy et al., 2008), and *Russellosaurus coheni* from the middle Turonian *Collignoniceras woollgari* Ammonite Zone, demonstrates significant diversification within basal plioplatecarpines as defined here, occurs within a mere ~1.5 million-year time span. Additionally, though all retain numerous plesiomorphic characters, there is significant morphological disparity in the snout, dermal palate, and braincase among these basal branching taxa.

The early cladogenesis of Plioplatecarpinae (as defined here) is matched by its longevity, persisting into the terminal Maastrichtian. Currently, the oldest tylosaurines known are from the middle Turonian *Prionocyclus hyatti* Ammonite Zone (~91Ma) of Texas (Polcyn et al., 2008; Bell et al., 2013), suggesting a ghost lineage for tylosaurines of at least 2.5 million years. The last tylosaurines are late Campanian or early Maastrichtian (e.g., Jagt et al., 2005). By comparison, the oldest known mosasaurine, *Dallasaurus turneri* (Bell and Polcyn, 2005), is from the middle Turonian *Collignoniceras woollgari* Ammonite Zone (~92.5Ma) and halisaurines appear in the fossil record in the Santonian (~85 Ma). This implies a ghost lineages for mosasaurines of about 1.5 million years, and nearly ten million years for halisaurines, those clades diverging in, or prior to, the early Turonian or possibly before (e.g. Mekarski et al., 2019), with representatives of both subfamilies persisting to the terminal Maastrichtian.

8. Conclusions

Herein we described and named a new mosasaur taxon, *Sarabosaurus dahli* gen. et sp. nov., from the *Watinoceras devonense* Ammonite Zone of the Tropic Shale, Utah. The holotype specimen is confidently dated at about 93.7 Ma based on radioisotopic dates from bentonites above and below the horizon from which it was preserved, and is thus the oldest named mosasaur taxon known from the Western Interior Seaway. Although the specimen exhibits numerous plesiomorphic traits, remarkably, the basisphenoid preserved with the specimen shows the derived plioplatecarpine basicranial circulation pattern, which is unique amongst squamates, and represents a key evolutionary novelty. We describe the basicranial circulation pattern in select mosasaurids, identifying a morphocline consisting of three types. We show the mosasaur subfamilies Tylosaurinae, Mosasaurinae, and Halisaurinae retain the plesiomorphic squamate condition (Type 1), while *de novo* vascular morphology supplants the basilar artery in *Tethysaurus* and *Russellosaurus* (Type 2), and the advanced plioplatecarpine (Type 3) condition is present in *Yaguarasaurus* and all other plioplatecarpines in which it can be assessed. Though some details remain unknown due to incomplete preservation of the basioccipital and the basisphenoid, *Sarabosaurus dahli* gen. et sp. nov. is inferred to possess the Type 3 condition because the basicranial canal for the basilar artery trends posteromedially within the basisphenoid as in later diverging plioplatecarpines. Recognition of the incipient (Type 2) condition in *Tethysaurus* and *Russellosaurus,* and the Type 3 condition in *Yaguarasaurus* and *Sarabosaurus dahli* gen. et sp. nov., provides the basis for an emended diagnosis of a more inclusive Plioplatecarpinae. The remarkable influence of these new data on the branching patterns recovered in our phylogenetic analysis, underscores the importance of discovery of new informative specimens, and the application of technology such as μCT in the search for new characters that elucidate the basal relationships and evolutionary patterns of mosasaurids.

Data availability

Data will be made available on request.

Acknowledgements

Many of the marine reptile specimens described from the Tropic Shale over the past several years were found by former Big Water residents D. Rankin and M. Graffam. We are pleased that they can now add mosasaurids to their list of discoveries. Our gratitude also extends to S. Richardson, who when given a request to find a mosasaur in the Tropic Shale by LBA under permit GLCA-2012-SCI-0006, went out and did just that – the type specimen, no less. J. Spence and S. Doyle at GLCA (and E. Clites formerly at GLCA) are thanked for their role in providing the permits required to collect fossils within Glen Canyon National Recreation Area and for their interest in our research; similar gratitude is extended to J. Kirkland and M. Hayden at the Utah Geological Survey for permission to search and collect on Utah state lands. T. Birthisel at UMNH (formerly at GSENM) helped in the field recovery and preparation of UMNH VP21800. For access to collections and assistance with specimens, we thank Jacques Gauthier, Dan Brinkman, and Marilyn Fox, Yale University; Anne Schulp and John Jagt, Natuurhistorisch Museum Maastricht; Dale Winkler, Shuler Museum of Paleontology at SMU; Annelise Folie, Royal Institute of Natural Sciences, Brussels,; Laura Wilson and Mike Everhart, Sternberg Museum of Natural History; Christopher Beard, University of Kansas; Mark Norell and Carl Mehling, American Museum of Natural History; Jun Ebersole, McWane Science Center, Birmingham AL; Adiel Klompmaker and Dana Ehret, Alabama Museum of Natural History. We thank Jason Anderson of the University of Calgary for access to the CT data, and Matt Colbert, Jessie Maisano HRCT lab at UTA and George D. Pylant III, for assistance with μCT scanning. We thank Louis Jacobs, Anne Schulp, Caitlin Keirnan and Bruno Augusta for comments on an earlier version of this manuscript. We thank Daniel Madzia and Joshua Lively for thorough and constructive reviews. The first author thanks ISEM at SMU (Southern Methodist University, Dallas, Texas, USA) for ongoing support of the Digital

Earth Science Lab (Huffington Department of Earth Sciences, SMU) and financial support for μCT scanning services.

References

Albright III, L.B., Gillette, D.D., Titus, A.L., 2007a. Plesiosaurs from the Upper Cretaceous (Cenomanian-Turonian) Tropic Shale of southern Utah, Part 1: new records of the pliosaur *Brachauchenius lucasi*. Journal of Vertebrate Paleontology 27, 31–40.

Albright III, L.B., Gillette, D.D., Titus, A.L., 2007b. Plesiosaurs from the Upper Cretaceous (Cenomanian-Turonian) Tropic Shale of southern Utah, Part 2: Polycotylidae. Journal of Vertebrate Paleontology 27, 41–58.

Albright III, L.B., Gillette, D.D., Titus, A.L., 2013. Fossil vertebrates from the Tropic Shale (Upper Cretaceous), southern Utah. In: Titus, A.L., Loewen, M.A. (Eds.), At the Top of the Grand Staircase, the Late Cretaceous of Southern Utah. Indiana University Press, Bloomington, pp. 536–562.

Albright III, L.B., Titus, A.L., Richardson, H.S., Clites, E.C., Birthisel, T.A., 2012. A basal mosasaurid from the lower Turonian (Upper Cretaceous) Tropic Shale of southern Utah. Journal of Vertebrate Paleontology, Programs and Abstracts 55.

Anan'eva, N.B., Orlov, N.L., 2013. Egg teeth of squamate reptiles and their phylogenetic significance. Biology Bulletin 40, 600–605.

Antunes, M.T., 1964. O Neocretácico e o Cenozóico do litoral de Angola. Junta de Investigações do Ultramar, Lisboa.

Augusta, B.G., Zaher, H., Polcyn, M.J., Fiorillo, A.R., Jacobs, L.L., 2022. A review of non-mosasaurid (dolichosaur and aigialosaur) mosasaurians and their relationships to snakes. In: Gower, D.J., Zaher, H. (Eds.), The Origin and Early Evolutionary History of Snakes. Cambridge University Press, Cambridge, UK, pp. 157–179.

Bardet, N., Suberbiola, X.P., Jalil, N.E., 2003. A new mosasauroid (Squamata) from the late Cretaceous (Turonian) of Morocco. Comptes Rendus Palevol 2, 607–616.

Bell Jr., G.L., 1997. A phylogenetic revision of North American and Adriatic Mosasauroidea. In: Callaway, J.M., Nicholls, E.L. (Eds.), Ancient Marine Reptiles. Academic Press, Cambridge, Massachusetts, pp. 293–332.

Bell, G.L., Polcyn, M.J., 2005. *Dallasaurus turneri*, a new primitive mosasauroid from the middle Turonian of Texas and comments on the phylogeny of Mosasauridae (Squamata). Netherlands Journal of Geosciences 84, 177–194.

Bell, G.L., Barnes, K.R., Polcyn, M.J., 2013. Late cretaceous mosasauroids (Reptilia, Squamata) of the Big Bend region in Texas, USA. Earth and Environmental Science Transactions of the Royal Society of Edinburgh 103, 571–581.

Blix, A.S., Walløe, L., Messelt, E.B., 2013. On how whales avoid decompression sickness and why they sometimes strand. Journal of Experimental Biology 216, 3385–3387.

Caldwell, M.W., Palci, A., 2007. A new basal mosasauroid from the Cenomanian (U. Cretaceous) of Slovenia with a review of mosasauroid phylogeny and evolution. Journal of Vertebrate Paleontology 27, 863–880.

Caldwell, M.W., Carroll, R.L., Kaiser, H., 1995. The pectoral girdle and forelimb of *Carsosaurus marchesetti* (Aigialosauridae), with a preliminary phylogenetic analysis of mosasauroids and varanoids. Journal of Vertebrate Paleontology 15, 516–531.

Camp, C.L., 1942. California mosasaurs, vol. 13. Memoirs of the University of California, pp. 1–68.

Cobban, W.A., Hook, S.C., 1984. Mid-Cretaceous molluscan biostratigraphy and paleogeography of southwestern part of the Western Interior, United States. In: Westermann, G.E.G. (Ed.), Jurassic-Cretaceous Biochronology and Paleogeography of North America. Geological Association of Canada Special Paper 27, pp. 257–271.

Cobban, W.A., Merewether, E.A., Fouch, T.D., Obradovich, J.D., 1994. Some Cretaceous shorelines in the western interior of the United States. In: Caputo, M.V., Peterson, J.A., Franczyk, K.J. (Eds.), Mesozoic Systems of the Rocky Mountain Region, USA. U.S. Geological Survey, Denver, Colorado, pp. 393–414.

Cobban, W.A., Walaszczyk, I., Obradovich, J.D., McKinney, K.C., 2006. A USGS zonal table for the Upper Cretaceous middle Cenomanian-Maastrichtian of the Western Interior of the United States based on ammonites, inoceramids, and radiometric ages. U.S. Geological Survey Open File Report, p. 2006, 1250.

Cope, E.D., 1869. On the reptilian orders, Pythonomorpha and Strep-tosauria. Boston Society of Natural History Proceedings 12, 250–266.

Cuthbertson, R.S., Maddin, H.C., Holmes, R.B., Anderson, J.S., 2015. The braincase and endosseous labyrinth of *Plioplatecarpus peckensis* (Mosasauridae, Plioplatecarpinae), with functional implications for locomotor behavior. The Anatomical Record 298, 1597–1611.

Cuthbertson, R.S., Mallon, J.C., Campione, N.E., Holmes, R.B., 2007. A new species of mosasaur (Squamata: Mosasauridae) from the Pierre Shale (lower Campanian) of Manitoba. Canadian Journal of Earth Sciences 44, 593–606.

Devillers, C., 1943. Nerfs craniens et circulation céphalique de "Plioplatecarpus Marshi". Annales de Paléontologie 30, 45–59.

Doelling, H.H., 1975. Geology and mineral resources of Garfield County, Utah. Utah Geological and Mineral Survey Bulletin 107, 175.

Doelling, H.H., Davis, F.D., 1989. The geology of Kane County, Utah, with sections on petroleum and carbon dioxide by Cynthia. J. Brandt. Utah Geological and Mineral Survey Bulletin 124, 192.

Dollo, L., 1882. Note sur l'ostéologie des Mosasauridae. Bulletin du Musee Royal d'histoire naturelle de Belgique 1, 55–80.

Dollo, L., 1885. Sur la presence d'un canal basioccipital median et de deux canaux hypobasilaires chez un genre de mosasaurien. Annales de la Societe Scientifique de Bruxelles 9, 309–338.

Dormer, K.J., Denn, M.J., Stone, J.L., 1977. Cerebral blood flow in the sea lion (*Zalophus californianus*) during voluntary dives. Comparative Biochemistry & Physiology 58, 11–18.

Dutchak, A.R., Caldwell, M.W., 2006. Redescription of *Aigialosaurus dalmaticus* Kramberger, 1892, a Cenomanian mosasauroid lizard from Hvar Island, Croatia. Canadian Journal of Earth Sciences 43, 1821–1834.

Dutchak, A.R., Caldwell, M.W., 2009. A redescription of *Aigialosaurus* (= *Opetiosaurus*) *bucchichi* (Kornhuber, 1901) (Squamata: Aigialosauridae) with comments on mosasauroid systematics. Journal of Vertebrate Paleontology 29, 437–452.

Dyman, T.S., Cobban, W.A., Davis, L.E., Eves, R.L., Pollock, G.L., Obradovich, J.D., Titus, A.L., Takahashi, K.I., Hester, T.C., Cantu, D., 2002. Upper Cretaceous marine and brackish water strata at Grand Staircase-Escalante National Monument, Utah. In: Lund, W.R. (Ed.), Field Guide to Geological Excursions in Southwestern Utah and Adjacent Areas of Arizona and Nevada. Field Trip Guide for the Geological Society of America Rocky Mountain Section, Cedar City, Utah, May 7-9, 2002, pp. 1–36.

Eaton, J.G., 1991. Biostratigraphic framework for the Upper Cretaceous rocks of the Kaiparowits Plateau, southern Utah. In: Nations, J.D., Eaton, J.G. (Eds.), Stratigraphy, Depositional Environments and Sedimentary Tectonics of the Western Margin, Cretaceous Western Interior Seaway. Geological Society of America Special Paper 260, pp. 47–63.

Elder, W.P., 1991. Molluscan paleoecology and sedimentation patterns of the Cenomanian-Turonian extinction interval in the southern Colorado Plateau. In: Nations, J.D., Eaton, J.G. (Eds.), Stratigraphy, Depositional Environments, and Sedimentary Tectonics of the Western Margin, Cretaceous Western Interior Seaway. Geological Society of America Special Paper 260, pp. 113–137.

Elderbak, K., Leckie, R.M., 2016. Paleocirculation and foraminiferal assemblages of the Cenomanian-Turonian Bridge Creek Limestone bedding couplets: productivity vs. dilution during OAE2. Cretaceous Research 60, 52–77.

Everhart, M.J., Pearson, G., 2014. An isolated squamate dorsal vertebra from the Late Cretaceous Greenhorn Formation of Mitchell County, Kansas. Transactions of the Kansas Academy of Science 117, 261–269.

Gale, A.S., Mutterlose, J., Batenburg, S., Gradstein, F.M., Agterberg, F.P., Ogg, J.G., Petrizzo, M.R., 2020. Chapter 27-The Cretaceous Period. In: Gradstein, F.M., Ogg, J.G., Schmitz, M.D., Ogg, G.M. (Eds.), Geologic Time Scale 2020. Elsevier BV, Amsterdam, Netherlands, pp. 1023–1086.

Georgi, J.A., 2008. Semicircular canal morphology as evidence of locomotor environment in amniotes. Doctoral dissertation. The Graduate School, Stony Brook University, Stony Brook, NY.

Gillette, D.D., Hayden, M.C., Titus, A.L., 1999. Occurrence and biostratigraphic framework of a plesiosaur from the Upper Cretaceous Tropic Shale of southwestern Utah. In: Gillette, D.D. (Ed.), Vertebrate Paleontology in Utah. Utah Geological Survey Miscellaneous Publication 99-1, Salt Lake City, pp. 269–274.

Grigoriev, D.V., Arkhangelsky, M.S., Kolchanov, V.V., Bulanov, V.V., Sennikov, A.G., Golubev, V.K., Skutschas, P.P., 2022. The use of zygapophyseal skeletochronology in individual age determination of a basal mosasauroid (Squamata, Mosasauridae) from the Campanian of Saratov Region. Paleontologicheskii Zhurnal 56, 441–447.

Hattin, D.E., 1985. Distribution and significance of widespread, time-parallel pelagic limestone beds in Greenhorn Limestone (Upper Cretaceous) of the central Great Plains and southern Rocky Mountains. In: Pratt, L.M., Kauffman, E.G., Zelt, F.B. (Eds.), Fine-grained Deposits and Biofacies of the Cretaceous Western Interior Seaway: Evidence of Cyclic Sedimentary Processes. Society of Economic Paleontologists and Mineralogists Midyear Field Trip Guidebook No. 4, 1985 Midyear Meeting, pp. 28–37.

Haq, B.U., 2014. Cretaceous eustasy revisited. Global and Planetary Change 113, 44–58.

Jagt, J.W.M., Lindgren, J., Machalski, M., Radwański, A., 2005. New records of the tylosaurine mosasaur *Hainosaurus* from the Campanian-Maastrichtian (Late Cretaceous) of central Poland. Netherlands Journal of Geosciences 84, 303–306.

Jones, M.M., Sageman, B.B., Oakes, R.L., Parker, A.L., Leckie, R.M., Bralower, T.J., Sepúlveda, J., Fortiz, V., 2019. Astronomical pacing of relative sea level during Oceanic Anoxic Event 2: preliminary studies of the expanded SH#1 Core, Utah, USA. Geological Society of America Bulletin 131, 1702–1722.

Kennedy, W.J., Walaszczyk, I., Cobban, W.A., 2005. The Global Boundary Stratotype Section and Point for the base of the Turonian Stage of the Cretaceous: Pueblo, Colorado, U.S.A. Episodes 28, 93–104.

Kennedy, W.J., Gale, A.S., Ward, D.J., Underwood, C.J., 2008. Early Turonian ammonites from Goulmima, southern Morocco. Bulletin de l'Institut Royal des Sciences Naturelles Belgique, Sciences de la Terre 78, 149–177.

Kier, E.L., Conlogue, G.J., VanHouten, J.N., 2022. Cerebral arterial and ventricular morphology of the dogfish (*Squalus acanthias*), American bullfrog (*Rana catesbeiana*), and green iguana (*Iguana iguana*): arterial high-resolution micro-CT, dissection, and radiography study. The Anatomical Record. https://doi.org/10.1002/ar.25028.

Konishi, T., Caldwell, M.W., 2011. Two new plioplatecarpine (Squamata, Mosasauridae) genera from the Upper Cretaceous of North America, and a global phylogenetic analysis of plioplatecarpines. Journal of Vertebrate Paleontology 31, 754–783.

Lillie, M.A., Vogl, A.W., Gerard, S.G., Raverty, S., Shadwick, R.E., 2022. Retia mirabilia: Protecting the cetacean brain from locomotion-generated blood pressure pulses. Science 377 (6613), 1452–1456.
Lindgren, J., Siverson, M., 2005. *Halisaurus sternbergi*, a small mosasaur with an intercontinental distribution. Journal of Paleontology 79, 763–773.
Lingham-Soliar, T., 1994. The mosasaur *Plioplatecarpus* (Reptilia, Mosasauridae) from the Upper Cretaceous of Europe. Bulletin de l'Institut Royal des Sciences Naturelles de Belgique, Sciences de la Terre 64, 177–211.
Mekarski, M.C., Japundžić, D., Krizmanić, K., Caldwell, M.W., 2019. Description of a new basal mosasauroid from the Late Cretaceous of Croatia, with comments on the evolution of the mosasauroid forelimb. Journal of Vertebrate Paleontology 39, e1577872.
Madzia, Cau, 2017. Inferring 'weak spots' in phylogenetic trees: application to mosasauroid nomenclature. PeerJ 5, e3782. https://doi.org/10.7717/peerj.3782.
Makádi, L., Caldwell, M.W., Ősi, A., 2012. The first freshwater mosasauroid (Upper Cretaceous, Hungary) and a new clade of basal mosasauroids. PLoS One 7, e51781.
Maisano, J.A., 2002. Postnatal skeletal ontogeny in five xantusiids (Squamata: Scleroglossa). Journal of Morphology 2541, 38.
Oelrich, T.M., 1956. The anatomy of the head of Ctenosaura pectinata (Iguanidae). University of Michigan Museum of Zoology Miscellaneous Publications 94, 1–122.
Palci, A., Caldwell, M.W., Papazzoni, C.A., 2013. A new genus and subfamily of mosasaurs from the Upper Cretaceous of northern Italy. Journal of Vertebrate Paleontology 33, 599–612.
Palci, A., Konishi, T., Caldwell, M.W., 2020. A comprehensive review of the morphological diversity of the quadrate bone in mosasauroids (Squamata: Mosasauroidea), with comments on the homology of the infrastapedial process. Journal of Vertebrate Paleontology 40, e1879101.
Paramo, M.E., 1994. Posicion sistematica de un reptil marino con base en los restos fosiles encontrados en capas del Cretacico superior en Yaguara (Huila). Revista de la Academia Colombiana de Ciencias Exactas, Fisicas y Naturales 19, 63–80.
Paramo, M.E., 2000. *Yaguarasaurus columbianus* (Reptila, Mosasauridae), a primitive mosasaur from the Turonian (Upper Cretaceous) of Columbia. Historical Biology 14, 121–131.
Petermann, H., Gauthier, J.A., 2018. Fingerprinting snakes: paleontological and paleoecological implications of zygantral growth rings in Serpentes. PeerJ 6, e4819.
Peterson, F., 1969. Cretaceous sedimentation and tectonism in the Kaiparowits region, Utah. United States Geological Survey Open-file Report 1314, 259.
Polcyn, M.J., Augusta, B., Zaher, H., 2022. Reassessing the morphological foundations of the pythonomorph hypothes. In: Gower, D.J., Zaher, H. (Eds.), The Origin and Early Evolutionary History of Snakes. Cambridge University Press, Cambridge, UK, pp. 125–156.
Polcyn, M.J., Bell Jr., G.L., Shimada, K., Everhart, M.J., 2008. The oldest North American mosasaurs (Squamata: Mosasauridae) from the Turonian (Upper Cretaceous) of Kansas and Texas with comments on the radiation of major mosasaur clades. Proceedings of the Second Mosasaur Meeting, Fort Hays Studies Special Paper 3, 137–155.
Polcyn, M.J., Bell, G.L., 2005. *Russellosaurus coheni* n. gen., n. sp., a 92 million-year-old mosasaur from Texas (USA), and the definition of the parafamily Russellosaurina. Netherlands Journal of Geosciences 84, 321–333.
Polcyn, M.J., Tchernov, E., Jacobs, L.L., 1999. The Cretaceous biogeography of the eastern Mediterranean with a description of a new basal mosasauroid from 'Ein Yabrud, Israel. In: Tomida, Y., Rich, T.H., Vickers-Rich, P. (Eds.), Proceedings of the Second Gondwanan Dinosaur Symposium, vol. 15. National Science Museum Tokyo Monographs, pp. 259–290.
Polcyn, M.J., Lindgren, J., Bardet, N., Cornelissen, D., Verding, L., Schulp, A.S., 2012. Description of new specimens of *Halisaurus arambourgi* Bardet and Pereda Suberbiola, 2005 and the relationships of Halisaurinae. Bulletin de la Societe Geologique de France 183, 123–136.
Polcyn, M.J., Jacobs, L.L., Araújo, R., Schulp, A.S., Mateus, O., 2014. Physical drivers of mosasaur evolution. Palaeogeography, Palaeoclimatology, Palaeoecology 400, 17–27.
Rahmat, S., Gilland, E., 2014. Comparative anatomy of the carotid-basilar arterial trunk and hindbrain penetrating arteries in vertebrates. The Open Anatomy Journal 6, 1–26.
Rieppel, O., 1993. Middle Triassic reptiles from Monte San Giorgio: recent results and future potential of analysis. Paleontologia Lombarda, ns 2, 131–144.
Rieppel, O., Zaher, H., 2000a. The braincases of mosasaurs and *Varanus*, and the relationships of snakes. Zoological Journal of the Linnean Society 129, 489–514.
Rieppel, O., Zaher, H., 2000b. The intramandibular joint in squamates and the phylogenetic relationships of the fossil snake *Pachyrhachis problematicus* Haas. Fieldiana (Geology), New Series 43, 1–69.
Russell, D.A., 1967. Systematics and Morphology of American Mosasaurs. Peabody Museum of Natural History Yale University Bulletin 23, 237.
Sageman, B.B., Meyers, S.R., Arthur, M.A., 2006. Orbital time scale and new C-isotope record for Cenomanian-Turonian boundary stratotype. Geology 34, 125–128.
Smith, K.T., Buchy, M.C., 2008. A new aigialosaur (Squamata: Anguimorpha) with soft tissue remains from the Upper Cretaceous of Nuevo León, Mexico. Journal of Vertebrate Paleontology 28, 85–94.
Sorenson, M.D., Franzosa, E.A., 2007. TreeRot, version 3. Boston University, Boston, MA.
Strong, C.R., Caldwell, M.W., Konishi, T., Palci, A., 2020. A new species of long-irostrine plioplatecarpine mosasaur (Squamata: Mosasauridae) from the Late Cretaceous of Morocco, with a re-evaluation of the problematic taxon 'Platecarpus' ptychodon. Journal of Systematic Palaeontology 18, 1769–1804.
Swofford, D., 2002. PAUP*: Phylogenetic Analysis Using Parsimony (*and Other Methods), Version 4. Sinauer Associates, Sunderland, MA.
Titus, A., Eaton, J., Sertich, J., 2016. Late Cretaceous stratigraphy and vertebrate faunas of the Markagunt, Paunsaugunt, and Kaiparowits plateaus, southern Utah. Geology of the Intermountain West 3, 229–291.
Venczel, M., Vasile, Ş., Csiki-Sava, Z., 2015. A Late Cretaceous madtsoiid snake from Romania associated with a megaloolithid egg nest–paleoecological inferences. Cretaceous Research 55, 152–163.
Viamonte, M., Morgane, P.J., Galliano, R.E., Nagel, E.L., McFarland, W.L., 1968. Angiography in the living dolphin and observations on blood supply to the brain. American Journal of Physiology, Legacy Content 214, 1225–1249.
Vogl, A.W., Fisher, H.D., 1982. Arterial retia related to supply of the central nervous system in two small toothed whales–narwhal (*Monodon monoceros*) an beluga (*Delphinapterus leucas*). Journal of Morphology 174, 41–56.
Wright, K.R., Shannon, S.W., 1988. Selmasaurus russelli, a new plioplatecarpine mosasaur (Squamata, Mosasauridae) from Alabama. Journal of Vertebrate Paleontology 8, 102–107.
Yi, H., Norell, M., 2018. The bony labyrinth of *Platecarpus* (Squamata: Mosasauria) and aquatic adaptations in squamate reptiles. Palaeoworld 28, 550–561.
Zippel, K.C., Lillywhite, H.B., Mladinich, C.R., 1998. Contribution of the vertebral artery to cerebral circulation in the rat snake *Elaphe obsoleta*. Journal of Morphology 238, 39–51.

Appendix A. Supplementary data

Supplementary data to this article can be found online at https://doi.org/10.1016/j.cretres.2023.105621.